Research Paper

PAIN®

OPEN

Altered pain sensitivity in 5×familial Alzheimer disease mice is associated with dendritic spine loss in anterior cingulate cortex pyramidal neurons

Zhengyu Cui[a,b], Zhongzhao Guo[a], Luyao Wei[a], Xiang Zou[c], Zilu Zhu[d], Yuchen Liu[d], Jie Wang[a], Liang Chen[c], Deheng Wang[d,*], Zunji Ke[a]

Abstract

Chronic pain is highly prevalent. Individuals with cognitive disorders such as Alzheimer disease are a susceptible population in which pain is frequently difficult to diagnosis. It is still unclear whether the pathological changes in patients with Alzheimer disease will affect pain processing. Here, we leverage animal behavior, neural activity recording, optogenetics, chemogenetics, and Alzheimer disease modeling to examine the contribution of the anterior cingulate cortex (ACC) neurons to pain response. The 5× familial Alzheimer disease mice show alleviated mechanical allodynia which can be regained by the genetic activation of ACC excitatory neurons. Furthermore, the lower peak neuronal excitation, delayed response initiation, as well as the dendritic spine reduction of ACC pyramidal neurons in 5×familial Alzheimer disease mice can be mimicked by Rac1 or actin polymerization inhibitor in wild-type (WT) mice. These findings indicate that abnormal of pain sensitivity in Alzheimer disease modeling mice is closely related to the variation of neuronal activity and dendritic spine loss in ACC pyramidal neurons, suggesting the crucial role of dendritic spine density in pain processing.

Keywords: Alzheimer disease, Chronic pain, ACC, Hypesthesia, Dendritic spine

1. Introduction

Pain acts as a warning signal to alert our body. The alterations in pain tolerance or sensitivity can be vital. The reduced pain sensitivity could alter the alert threshold of myocardial infarction or fractures.[10,19,71]

Alzheimer disease (AD) is the most common dementia. Half of the patients with AD suffer from pain,[48] but how to assess pain intensity is a big challenge: disorder of pain recognition and communication disabilities. Participants with a higher ability to communicate are found more likely to receive better pain treatment.[9,45] Conflicting to the fact that fewer analgesics drugs are administrated in patients with AD, much more brain regions were activated in the functional magnetic resonance imaging (fMRI) test.[13] A placebo-controlled trial of paracetamol application shows no positive effect in patients with advanced dementia, indicating the requirement of a proper assessment and monitoring approach.[82] Several methods of designing reliable evaluation criterion were proposed but proved very little success.[15,47,62]

The cingulate cortex has been implicated in the regulation of many advanced cognitive functions, such as attention, emotion, and sensory processing.[1,17,63] Increasing evidences of brain imaging studies have identified the function of anterior cingulate cortex (ACC) about sensing the acute nociception.[38,84] Alterations of neuronal activity in ACC are found in patients with chronic pain, which indicates the possible relationship between them.[18,22,39] Peripheral inflammation triggers temporal imprecision of information coding in the ACC neurons.[41] The putative pyramidal neurons are nociceptive to the contralateral hind paw mechanoreception.[35] Furthermore, the neuronal activity modulated by optogenetic techniques can regulate the pain threshold in complete Freund adjuvant (CFA)-induced hypersensitive modeling mice.[34]

The mature-shaped spine provides essential biochemical and electrical compartmentalization within neurons which keeps the postsynaptic density of excitatory synapses.[27,53,92] One of AD pathogenesis is believed to be driven by structural synaptic modifications and compromised synaptic transmission induced by Aβ toxicity.[60,66,67,96] Aβ may be associated with the increased inhibitory modulation in the spinal cord and aberrant activation of striatal enriched protein tyrosine phosphatase signaling in hippocampi.[3,40] Synaptic damage is usually found in patients with AD with cognitive

Sponsorships or competing interests that may be relevant to content are disclosed at the end of this article.

D. Wang and Z. Ke contributed equally to this work.

[a] Academy of Integrative Medicine, Shanghai University of Traditional Chinese Medicine, Shanghai, China, [b] Department of Internal Medicine of Traditional Chinese Medicine, Shanghai East Hospital, Tongji University, Shanghai, China, [c] Department of Neurosurgery, Huashan Hospital, Fudan University, Shanghai, China, [d] Department of Physiology, School of Basic Medical Sciences, Shanghai University of Traditional Chinese Medicine, Shanghai, China

**Corresponding author. Address: Shanghai University of Traditional Chinese Medicine, 1200 Cailun Rd, Shanghai 201203, China. Tel.: +86-21-51323172; fax: +86-21-51323172. E-mail address: wangdeheng@shutcm.edu.cn (D. Wang).*

Supplemental digital content is available for this article. Direct URL citations appear in the printed text and are provided in the HTML and PDF versions of this article on the journal's Web site (www.painjournalonline.com).

PAIN 163 (2022) 2138–2153

http://dx.doi.org/10.1097/j.pain.0000000000002648

defect, as well as the synaptic degeneration in 5×familial Alzheimer disease (FAD) mice.[32,88] Spine morphodynamics is proved closely related to changes of F-actin-rich cytoskeleton, which are regulated by Rho-GTPases.[36] Recent researches have reported that the aberrant F-actin depolymerization and Rac1 levels decrease in adult AD mice.[7,37] Administration of Rac1-inhibitor or actin polymerization inhibitor[58] may modulate neurotransmission by reducing the spine density.[74,75] Here, we hypothesize that the dysgenesis and instability of the dendritic spine in ACC may lead to hypesthesia in inflammatory pain.

In this study, we discovered the AD pathology that came with the reduction of pain response in 5×FAD mice. As the neuronal activity is closely related to dendritic spine density,[2,29,65,72] *in vivo* electrophysiology studies revealed dendritic spine loss in ACC can be the key information to induce the behavioral and neuronal activity change. Taken together, our results demonstrate that the alteration of dendritic spine density in AD may result in the hypesthesia of chronic pain.

2. Materials and methods

2.1. Ethics statement

All experiments in the study involving living animals were approved by the Institutional Animal Care and Use Committee at Shanghai University of Traditional Chinese Medicine, Shanghai, China.

2.2. Subjects

Adult (3-, 6-, and 9-m old) male wild-type (WT, C57/BL6J) and 5×FAD (Nanjing University—Nanjing Institute of Biomedicine, No. 201400975) mice were used. Only male gender is applied in this study to eliminate the effect of estrogen to pain processing by different age.[94] Mice had free access to food and water and were group housed on a 12/12 hours light or dark cycle (4-5 animals per cage) at a constant temperature (24 ± 1°C) and humidity (50 ± 5%). All experiments were conducted during the light cycle. Littermates were randomly assigned to each condition by the operator.

2.3. Behavioral tests

During the scoring of all behavioral tests (von Frey test, CatWalk gait analysis, and Hot plate test), the experimenters were blinded to the genotype of the mice.

2.4. Complete Freund adjuvant–induced paw inflammation

The paw inflammation was induced by intraplantar injection of 20 μL CFA (diluted 1:1 with 0.9% saline; Sigma-Aldrich, St. Louis, MO) in the von Frey test and CatWalk gait analysis. The animals were anesthetized by 1% pentobarbital sodium (10 mg/kg), and ipsi-injected paw circumference (max coil perimeter of the hind limb) was measured immediately before and 3 hours after CFA injection.

2.5. Mechanical pain measurement (von Frey test)

Mice were habituated for 1 hour in a small clear acrylic box (15 × 15 × 15 cm) atop mesh flooring. We applied 7 different intensities of von Frey filament stimulus (Aesthesio, Campbell, CA) ranging from 0.16 to 4 g. Starting from the lowest intensity, each filament which applied 5 trials was used to poke the plantar surface of animal's hind paw until the filament bent. The percentage of paw withdrawal was calculated for each filament (withdrawal trials/total trials). Pain threshold refers to the withdrawal rate > 50%. von Frey tests were repeated at 4, 24, 48, and 72 hours after CFA injection.

During the trails of in vivo recording, optogenetic or chemogenetic manipulation, and dendritic spine density inhibition, 2 filaments (1.4 and 0.6 g) were chosen to perform the von Frey tests. The paw withdrawal percentage induced by 1.4 g filament stimuli was acquired 4 hours before CFA injection. The paw withdrawal percentage induced by 0.6 g filament stimuli was acquired 4 hours after CFA injection. Each filament was applied for 10 times with intervals more than 5 minutes.

2.6. CatWalk gait analysis

The CatWalk system consists of an enclosed walkway (glass plate) in which a rodent can move from one side of the walkway to the other. The digital frame was recorded by a video camera. The pixel value of a digital frame is determined by the brightness value. The Illuminated Footprints technology allows for an accurate distinction between different paws that make contact with the glass floor. The mean intensity value acquired before CFA injection is considered the baseline value, whereas the relative value refers to the proportion of the real-time measurement value divided by the baseline value. By following the timeline in **Figure 1A**, the mice were conducted 3 trials per day to collect the data. CatWalk tests were repeated 4, 24, 48, and 72 hours after CFA injection.

2.7. Hot plate test

A plate metal was placed flatwise on a hotplate and heated to 55°C. Mice were placed on the hotplate, and the paw withdrawal latency was recorded by researchers. The shift duration results from subtracting 2 durations (after CFA − before CFA). We compared the shift latency duration between 5×FAD and WT group per age. All sessions were video recorded.

2.8. Virus construction

AAVs particles (AAV2/9-mCaMKIIa-hChR2(H134R)-mCherry-WPRE-pA, titer, 2.5×10^{12}gc·ml^{-1}; AAV2/9-mCaMKIIa-hM4D(Gi)-mCherry-WPRE-pA, titer, 2.5×10^{12}gc·ml^{-1}) were purchased from Taitool, Shanghai, China.

2.9. Stereotaxic injection

The animals were anesthetized and placed in a stereotactic frame (RWD, Shenzhen, China). For optogenetic activation of glutamatergic neurons in ACC (opposite side of the CFA injection: anterior-posterior [AP]: +0.4 mm, medial-lateral [ML]: 0.5 mm, and dorsal-ventral [DV]: 1 mm), 300 nL of AAV2/9-mCaMKIIa-hChR2(H134R)-mCherry virus was injected by a 10-μL Hamilton microsyringer (Hamilton Co.) at a constant speed of 30 nL/min (PUMP 11 ELITE Nanomite; Harvard Apparatus, Holliston, MA). After viral injection, the needle was kept for 10 minutes to ensure the diffusion of the virus. The needle was then withdrawn slowly and completely.

For chemogenetic suppression, 300 nL of AAV2/9-mCaMKIIa-hM4D(Gi)-mCherry virus was injected which follow the same method.

2.10. Tetrode electrode construction and implantation surgery

Self-made headstages were constructed using the procedures which we published previously.[70,87] Four wires (California Fine

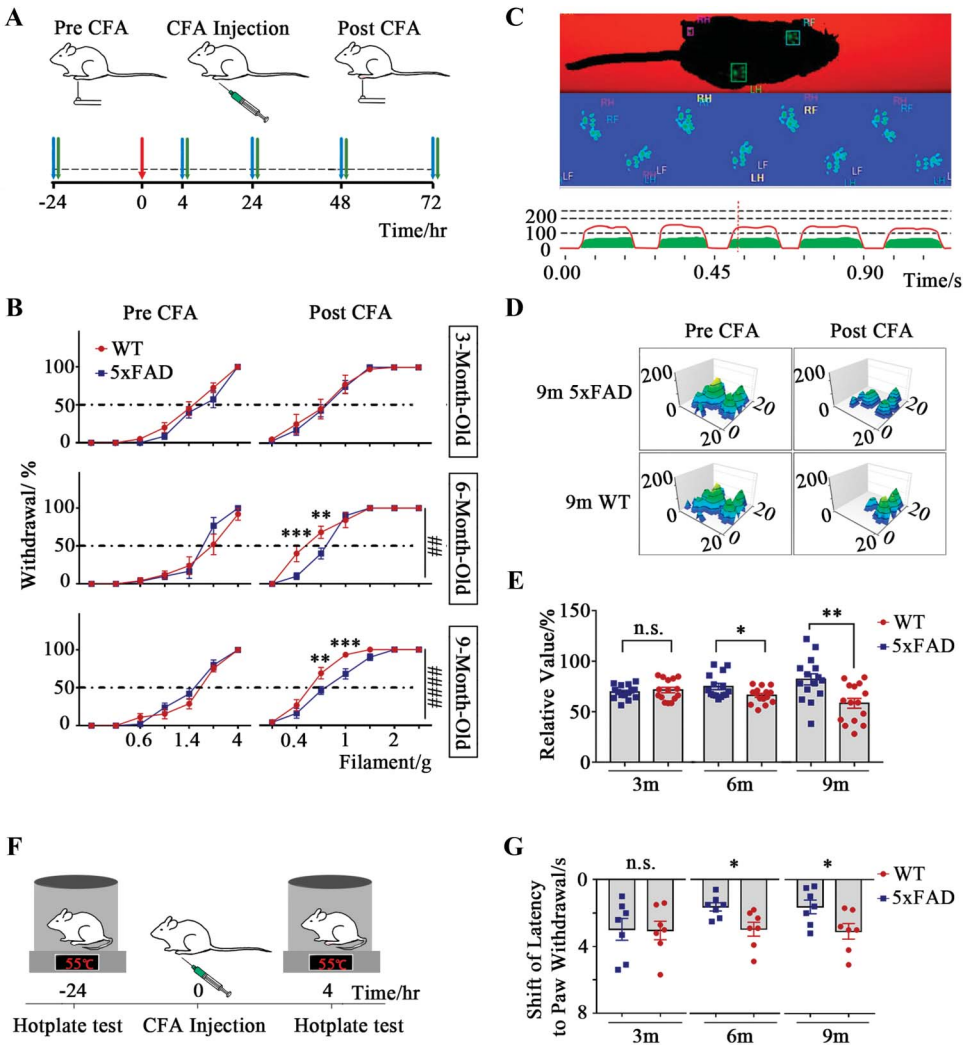

Figure 1. Reduced mechanical and heat pain responses in 5×FAD mice. (A) Schematic of CFA injection and von Frey test (top, intraplantar injection in left hind paw after the von Frey test). Timeline of the behavioral tests including gait analysis (blue arrows) and von Frey test (green arrows). Time zero: CFA injection (red arrow) (bottom). (B) The paw withdrawal percentage of all groups before and 4 hours post-CFA injection (3 m: 5×FAD, n = 8; WT, n = 7) (top), (6 m: 5×FAD, n = 6; WT, n = 5) (middle), (9 m: 5×FAD, n = 10; WT, n = 9) (bottom) (5×FAD vs WT: $^{*}P < 0.05$; $^{**}P < 0.01$; $^{***}P < 0.001$; $^{****}P < 0.0001$, unpaired Student *t* test). Two-way ANOVA was performed after CFA to investigate the effects of genotype at 6 m mice ($F(2, 91) = 6.593$, $\#\#P = 0.0021$) and 9 m mice ($F(1, 119) = 17.29$, $\#\#\#\#P < 0.0001$). (C) 2D Footprint of a representative mouse walking in the CatWalk gait analysis maze (top). The solid red line represents the maximum intensity, whereas the filled green area under the red line represents the mean contact intensity of the paw (bottom). (D) Representative images of instantaneous hind paw pressure intensity and area of hind paw contact before and 4 hours post-CFA injection. (E) Relative values of inflamed paw (Mean intensity$^{post\text{-}CFA}$/Mean intensity$^{pre\text{-}CFA}$) at 24 hours, 48 hours, and 72 hours after CFA in WT and 5×FAD mice. 3 m, 6 m, and 9 m each group: n = 15 (5×FAD, n = 15; WT, n = 15), (5×FAD, n = 15; WT, n = 15), and (5×FAD, n = 15; WT, n = 15) (Each groups vs baseline: $^{*}P < 0.05$; $^{**}P < 0.01$, unpaired Student *t* test). (F) Experimental design (CFA injection and hotplate test), mice were injected with CFA after a baseline hotplate test and tested again 4 hours after CFA injection. (G) Shift of latency to paw withdrawal in the hotplate test (post-CFA – pre-CFA) compared between 5×FAD and WT group (n = 7 per group, unpaired Student *t* test, $P < 0.05$). ANOVA, analysis of variance; CFA, complete Freund adjuvant; FAD, familial Alzheimer disease; WT, wild type.

Wire Company, Grover Beach, CA) were twisted together, and the insulating layer was melted by a low-intensity heat gun. Then, the twisted wires were threaded into polymicro capillary tubing (Polymicro Technologies, Phoenix, AZ). The impedances of each channel of headstages were measured with an impedance tester (Nano-Z, Plexon, Dallas, TX). The typical impedances were between 0.5 and 1 MΩ. The tips of wires were cut to fit the recording depth and to prevent oxidation.

The animals were handled for minimal 3 days before electrode implantation surgery. After handling, the animals were anesthetized and placed on the stereotactic frame (RWD). We used the movable bundles of the 32-channel electrode to target the ACC (opposite side of the CFA injection: AP +0.4 mm; ML 0.5 mm and DV 1 mm) and S1 (opposite side of the CFA injection: AP -0.2 mm, ML 1.8 mm, and DV 0.3 mm). To eliminate the possible effect of anaesthesia on the neural activity and allow sufficient recovery time, mice were placed at homecage for at least 1 week before neural recording.

2.11. In vivo single-unit recording and data sorting

We used the tetrode electrode to record the single-unit activity in freely behaving mice (WT and Alzheimer disease: both n = 10). The animals were given 3 to 7 days to recover from the electrode implantation surgery. Multichannel extracellular signals were recorded during von Frey filament stimulation from the ACC (opposite side of the CFA injection: AP +0.4 mm, ML 0.5 mm, and DV 1 mm). Drivable microelectrode was advanced around 35 μm daily until we could record the maximal units. The signals were amplified, band-

pass filtered (0.5-1000 Hz for local field potentials [LFPs] and 0.6-6 kHz for spikes), and digitized using the Plexon OmniPlex Neural Data Acquisition System (Plexon, Dallas, TX). Spikes detected at adjustable online thresholds were collected at 40 kHz. Signal units were clustered in Offline Sorter and Mclust 4.4 program (A. D. Redish, http://redishlab.neuroscience.umn.edu/MClust/MClust.html).

2.12. Single-unit data analysis

Peristimulus time histogram for the time point of the filament bents is computed with 100 ms between −5 and 10 seconds relative to the time for each neuron. To calculate the z-score firing rate, we used the following equation:

$$Z-\text{score} = \frac{FR-\mu}{\sigma} \quad (1)$$

FR indicates the immediate firing rate (bin), and μ indicates the mean baseline firing rate before filament stimulus. σ is the standard deviation of μ. The means and standard deviation of baseline was calculated from 60 seconds before stimulus. To define a responsive neuron, we use the following criteria: (1) the absolute value of the z-score firing rate of minimal 5 bins after stimulation must be ≥ 2.33, and (2) if the first rule is met, the minimum z score (Z_{bin}) as calculated by ($Z_{bin} - Z_{SEM}$) at least 2 bins after stimulation must be larger than 1.645. Z_{SEM} refers to the following equations:

$$ZSEM\ (bin) = \frac{FRSEM(bin)}{\text{Standard Deviation of } \mu} \quad (2)$$

The FR_{SEM} (bin) = (standard error of FR over all filament trials)/bin size. For ACC neurons that demonstrated increased firing rate before or after CFA injection, we also used a robust linear regression model to fit the peak z-score firing rates in response to after or before CFA and to analyse the slope. We use the regression line to distinguish between pre-CFA stimulus and post-CFA stimulus. For comparing the slopes of regression lines, we used the Student *t* test. If the value of $P < 0.05$, we considered that it is statistically significant.

2.13. Local field potential recording and data analysis

The LFP value refers to the real-time potential under the sampling frequency of 1000 Hz. Peristimulus LFP voltage change was calculated with bins of 500 ms between 3 seconds before and 3 seconds after filament poke. To calculate the representative time point, by using the analysis software of NeuroExplorer Version 5.306 (Nex Technologies, Madison, Alabama), we compare the values in 0.5, 1, 1.5, 2, 2.5, and 3 seconds with baseline. Baseline refers to the average value calculated 3 seconds before filament stimulus.

2.14. Measurement of optic fiber transmissivity

Light intensity was measured at laser launch, tip of coupled fiber (diameter, 200 μm; Ferrule O.D, 1.25 mm; N.A., 0.37; and length, 4 mm; Inper, Inc, Hangzhou, Zhejiang, China). Fiber ferrules were sorted based on optical transmissivity (>80%). We measured light intensity before connecting to the implanted fiber ferrule. In addition, the intensity was kept to adjust to certain power (ChR2 stimulation: 1 mW).

2.15. Optogenetic and chemogenetic manipulation

We use 2 genetic manipulations to 5×FAD and WT mice. For 5×FAD mice, we used the optical stimulation in which the laser light (450 nm) was delivered to the ACC brain region for 3 hours after CFA injection. The optogenetic stimulation lasted for 1 second at 0.1 Hz (1 stimulus every 10 seconds).

The baseline z score was calculated from the 60 seconds before laser stimulus. The time window (bin size) for z-score calculation is 100 ms. We selected the units which response to laser stimulus as well as the filament stab to analyse the von Frey test–induced z-score change after CFA injection. The WT mice were injected intraperitoneal of clozapine-N-oxide (CNO, 2.5 mg/kg) to confirm the inhibition of glutamatergic neurons in ACC.

2.16. Immunostaining and cell counting

Mice were anesthetized with pentobarbital sodium (1%, 10 mg/kg) 5 hours after CFA intraplantar injection and perfused transcardially with 0.9% sterile saline followed by ice-cold 4% paraformaldehyde. The brain was removed carefully and placed into the 4% paraformaldehyde at 4°C overnight, then cryoprotected in Phosphate buffered saline (PBS) containing 30% sucrose for 24 hours. Coronal sections were sliced into 35 μm by using Leica cryostat (Wetzlar, Hesse, Germany). Free floating sections were rinsed with PBS on a shaker (60 rpm, 10 minutes ×3 times) and incubated in 0.3% TritonX-100 and 10% normal goat serum (Jackson, West Grove, PA) in PBS for 1 hour at room temperature. Primary antibody against c-fos (a marker of neuronal activity) (1:400, sc-52; Santa Cruz Biotechnology, Dallas, TX), NeuN (dilution 1:200, 2625391; Millipore, Billerica, MA), or CaMKII (1:250, ab22609; Abcam, Cambridge, United Kingdom) dissolved in blocking solution (1% bovine serum albumin and 0.1% TritonX-100) was applied overnight at 4°C. Negative controls were conducted by omitting the primary antibody. We did not detect non-specific labeling in negative controls. After thorough washing with PBS, the sections were incubated with secondary antibodies at room temperature for 2 hours. The antibodies were Alexa fluor 488 or 594 goat anti-rabbit IgG and Alexa fluor 488 or 594 goat anti-mouse IgG (1:100, Jackson). After washing with PBS (10 minutes × 3 times), the sections were mounted on gelatin coated and cover slipped with an antifade reagent and DAPI (Image-iT FX Signal Enhancer; Invitrogen, Carlsbad, CA). The sections were then photographed and analyzed with a Leica TCS SP5 laser scanning confocal microscope.

To determine the quantification of calmodulin-dependent protein kinase II^+ ($CaMKII^+$) and $c\text{-}fos^+$ neurons in ACC or S1, 3 coronal sections per mouse from the unilateral region (ACC: AP from 0.2-0.6 mm, S1: AP from 0 to −0.4 mm spaced 200 μm apart) were examined. Cells were counted manually by 3 research assistants who were blinded to the experimental condition in midst of the corresponding regions by using Image J (NIH).

2.17. Thioflavine S staining

We performed analysis on Aβ deposits by comparing the size of the green fluorescence area. 3 coronal sections were selected per mouse. All of the sections were stained in parallel. We count the Aβ area % by dividing the Aβ deposit area into the whole ACC area.

2.18. Golgi staining, spine counting, and morphological analysis

Morphologic features of ACC pyramidal neurons were visualized by using the FD Rapid Golgi Stain kit (manufacturer's protocol, FD NeuroTechnologies, Columbia, MD). Dendritic morphology and

spine configuration were reconstructed and analyzed using Imaris software (version 7.7.2). For dendritic complexity analysis and spine density calculation, the brains were coronally sectioned at 100 μm thickness with a vibratome (VT1000S; Leica, Germany) and placed on glass slides which were covered by 1% gelatin. Only fully impregnated pyramidal neurons that reserved entirely soma were used. A Zeiss microscope with a motor stage equipped with transducers on the XYZ axes was used to trace each neuron at low magnification (×20) for dendritic tree reconstruction and at high magnification (100× oil objective) for spine reconstruction at 0.50 μm or 1 μm increments. Image z stacks were taken every 0.15 mm at a resolution of 1024 × 1024 pixel, yielding an image with pixel dimensions of 49.25 × 49.25 mm. All images were taken by an operator who was blinded to the genotype of the brain slices.

Dendritic tracing originated from soma having diameters ranging from 6 to 12 μm and terminated once the dendrite diameters were smaller than 0.6 μm. Sholl analysis was then performed on the 3-dimensionally reconstructed neurons to calculate the numbers of intersections per each Sholl ring (10 μm intervals) to gather information on the changes in dendritic tree complexity.

Z-stack image contrast was inverted using the Imaris software. At least 30 dendrites from at least 5 mice per genotype were counted. For spine morphology analysis, we analyzed between 600 and 900 spines (120 spines per mouse from at least 5 mice per genotype). Twenty to 30 consecutive spines on the same dendrite were analyzed per image.

Spine subtypes were analyzed based on previously defined morphological criteria[26,93] and quantitated as follows: (1) mushroom: the spine head diameter is ≥ 1.5 × the diameter of spine neck ($d_h/d_n \geq 1.5$), (2) stubby: head and neck of the spine are approximately of the same width and spine length is not significant longer than the bead diameter ($d_h/d_n < 1.5$ and $L/d_h < 2$), (3) thin: diameters of spine head and neck are much the same and spine length is greater than spine width ($d_h/d_n < 1.5$, $L/d_h > 2$), and (4) branched: spines with more than one head. Mature spine consists of mushroom subtype and stubby subtype.

2.19. Lateral ventricle catheterization and drug delivery

Owing to the higher survival rates in vivo, the lateral ventricle injection was chosen to deliver the drug. The mouse is anesthetized and fixed in the stereotaxic apparatus (RWD). The catheter consists of a polyethylene pipe (inner diameter: 0.2 mm and outer diameter: 0.25 mm) imbedded by the microsyringe (AP: −0.7 mm, ML: 1.5 mm, and DV: 2 mm). During the injection process, an artery occlusion is applied at the stem of poly ethylene, to ensure the air impermeability of the equipment. The speed of injection is 40 nL/min, and the total volume is 0.4 μL. After injection is completed, the needle is held for 5 minutes to prevent the fluid backflow. Then, a 0.2 mm diameter metal wire was inserted into the polyethylene pipe after the needle withdrawal to prevent the spillage of cerebrospinal fluid (CSF). 0.9% sterile saline or NSC23766 trihydrochloride (NSC) (10 mg/mL, ab142161; Abcam, Cambridge, United Kingdom) is infused through the catheter for 3 days (0.4 μL volume; twice a day) in NSC treatment experiment. 0.9% sterile saline or cytochalasin D (CD) (25 mg/mL, ab143484; Abcam) is infused for 3 days (1 μL volume; twice daily) in CD treatment experiment.

2.20. Data processing and statistical analysis

We use the GraphPad Prism 7 software program to generate figures and analyze data. Data are shown as mean ± SEM. Paired or unpaired Student *t* tests were performed to compare the data with 2 experimental groups. Analysis of variance followed by the Tukey post hoc test was used in multiple groups. A value of $P \leq 0.05$ was defined statistically significant.

2.21. Data availability

The data that support the findings of this study are available from the corresponding author on reasonable request.

3. Results

3.1. Pathological changes in 5×familial Alzheimer disease mice alleviate the mechanical and thermal pain

To understand how Alzheimer disease influences inflammatory allodynia, the mechanical and thermal thresholds in mice with different ages are observed. The paw withdrawals induced by noxious stimulus are related to spinal reflexes which have been proved similarly at different stimulating intensities.[83] Symptom of that foot swelling after CFA intraplantar injection usually occurs (Supplementary Fig. 1A, available at http://links.lww.com/PAIN/B618). To eliminate the influence of inflammatory swelling on the paw withdrawal rate, the paw circumference measurements were performed. No significant difference of paw circumference was found between 5×FAD and WT mice (Supplementary Fig. 1B, available at http://links.lww.com/PAIN/B618). The mechanical filament pain thresholds of both WT and 5×FAD mice were measured at 24 hours before CFA and 4, 24, 48, and 72 hours after CFA (**Fig. 1A**). Both of the WT and 5×FAD animals exhibited mechanical hypersensitivity after the CFA-induced inflammation. Furthermore, the 6/9-m 5×FAD mice showed reduced paw withdrawal rate which implied the alleviated pain response (**Fig. 1B**). The hypesthesia phenomenon fades away after 24 hours post-CFA in the 6-m 5×FAD mice whereas the 9-m 5×FAD mice last for 48 hours (Supplementary Fig. 1C, available at http://links.lww.com/PAIN/B618).

To assess the pain response in inflammatory condition further, the CatWalk behavioral test was performed (**Fig. 1C** top). The green signal which measures the intensity of paw pressure in real time appears only at the time the paws touch the floor (**Fig. 1C** bottom). The mean intensity of the paw press on the floor, reflecting the lower withdrawal threshold in nerve injury,[33,89] was computed over the whole stance period (**Fig. 1D**).[86] The relative value of paw pressure mean intensity ($\text{Mean intensity}^{\text{Post-CFA}}/\text{Mean intensity}^{\text{Pre-CFA}}$) in 5×FAD was higher than WT mice at 6-m-old and 9-m-old groups 4 hours after CFA injection (**Fig. 1E**). However, no difference was found at 24, 48, and 72 hours after CFA in WT and 5×FAD mice (Supplementary Fig. 1D, available at http://links.lww.com/PAIN/B618). To verify whether 5×FAD or WT mice are resistant to age-related increases in chronic pain development, we compared the withdrawal percentage 4 hours after CFA injection from identical genotype between different months. Both of WT and 5×FAD mice show no significant difference among 3/6 or 9 month old (Supplementary Fig. 1E, F, available at http://links.lww.com/PAIN/B618).

To determine whether the thermal pain threshold changed in 5×FAD mice just as mechanical pain threshold, we next explore how CFA injection influences the withdrawal latency by the hotplate test. We compared the shift of latency to paw withdrawal ($\text{Latency}^{\text{post-CFA}} - \text{Latency}^{\text{pre-CFA}}$) between WT and 5×FAD mice (**Fig. 1F**). The result shows that 5×FAD mice decreased significantly than WT mice at 6 and 9 m old, which may imply the reduced thermal pain response under inflammatory condition in AD models (**Fig. 1G**).

3.2. Delayed firing initiation and lower excitability in anterior cingulate cortex putative pyramidal neurons of 5×familial Alzheimer disease mice

Anterior cingulate cortex plays a vital role in pain and emotion modulation.[84] Human brain fMRI studies also showed that ACC is consistently and obviously activated by pain.[38] Neuropathological alterations are most likely to be detected at 4-m AD modeling mice[69,88]; our study which is trying to uncover the potential mechanism of chronic pain in AD modeling animal is conducted on 3 and 6 m mice because the AD mice of 6 m and 9 m groups both show altered pain response in von Frey filament stimulation, thermal test, and CatWalk analysis which support that the 6-m group may represent the AD modeling mice with neuropathological features. We use the multichannel in vivo recording technique to monitor the neurons in layer IV/V of contralateral ACC (**Fig. 2A**). Action potential and LFP are recorded and then analyzed by Offline Sorter, NeuroExplorer software (**Fig. 2B**), and MATLAB custom written code. By applying different intensity filament stimulus, we noticed that the voltage of LFP is related to the intensity of stimulus in each group at 6 m. The 1.0 g stimulus could evoke the neuronal activity increased earlier than 0.6 g stimulus, whereas the 1.4 g stimulus induced the maximum amplitude and the earliest firing change (**Figs. 2C and D**). Primary somatosensory cortex (S1) is also correlated with subjective pain perception and involved in AD pathology.[57,77,78] A similar phenomenon of LFP change in the S1 brain area under different intensity filament stimulations was observed (Supplementary Fig. 2A, available at http://links.lww.com/PAIN/B618), but only 2 time points show significant change compared with the ACC brain (1 and 1.4 g filaments stimulus, Supplementary Fig. 2B, available at http://links.lww.com/PAIN/B618). Increased expression of c-fos, an immediate early gene protein product, is a hallmark of ACC neurons undergoing nociception.[42] To further deepen our understanding of neuronal excitation condition in AD models, we compared c-fos expression 5 hours after CFA injection in ACC (**Figs. 2E and F**) and S1 (Supplementary Fig. 2C, D, available at http://links.lww.com/PAIN/B618). Interestingly, the c-fos$^+$ nucleus is reduced at the age of 6 and 9 m AD models in ACC (**Fig. 2G**) but not in S1 (Supplementary Fig. 2E, available at http://links.lww.com/PAIN/B618).

A 1.4 g filament poke, a noxious stimulus to mice, is sufficient to activate C-fiber and A-fiber mechanonociceptors in electrophysiological studies.[81,90] Different intensities of filament stimulus were tested to decide which filament to use before or after CFA. When several forces of filaments were chosen to compare the pain response between pre-CFA and post-CFA in WT and AD mice, 50% mechanical nociceptive threshold drops to around 0.6 g in inflamed mice from 1.4 g before CFA. In this case, the von Frey 1.4 g stimuli 4 hours pre-CFA and 0.6 g stimuli 4 hours post-CFA were selected to test evoked neuronal activity across naïve and CFA-treated groups at 3 and 6 m mice (**Fig. 3A**). Not surprisingly, both the WT and AD group with implanted electrodes showed the same withdrawal percentage as the groups without electrode which indicated the electrode implantations have no effect to the behavior tests (**Fig. 3B**). We managed to collect enough well-isolated neurons from 3-m and 6-m 5×FAD and WT (**Figs. 3C and D**). These units were classified based on the characteristic of firing rate, waveform, interspike interval (Supplementary Figs. 3A, B, available at http://links.lww.com/PAIN/B618), excitability, and responsive duration (Supplementary Figs. 3C, D, available at http://links.lww.com/PAIN/B618). For neuronal spike analysis, to define a responsive unit, we calculate the perievent time histograms of 5 seconds before and 10 seconds after filaments' stimuli with 100 ms bin size. The baseline (red dotted line) is calculated as the mean value of the 60 seconds prior stimuli. The excitatory or inhibited units (red thick solid line neurons) are classified by z-scored variation. To determine how the neuronal activity changes, each of the neurons we analyzed should be recorded at least 12 hours (from 4 hours pre-CFA to 8 hours post-CFA). Based on our definition, 19.23% of total recorded neurons of 3-m 5×FAD mice, 16.41% of 3-m WT mice, 29.55% of 6-m 5×FAD and 25.58% of 6-m WT are classified as responsive excitatory units (**Figs. 3C and D**). No significant difference in initiations of firing was found between 3-m 5×FAD and WT mice (**Figs. 3E and F**), whereas it was significantly delayed in 6-m 5×FAD mice compared with the same age WT control (**Figs. 3G and H**). We then examined the "tuning curves" of all ACC neurons that showed increased peak firing rates of post-CFA than pre-CFA. Such tuning curves demonstrate the degree of neuronal responses to different intensities of filament stimulation. The data of 6-m 5×FAD group show a flatter tuning curve which indicated a significant decrease in the slope of linear fit, suggesting a weak neuronal response to inflammatory stimuli (**Figs. 3I and J**). Together with the lower limb withdrawal percentage in 5×FAD mice, these data may suggest that the ACC neural activity may correlate with the pain severity in AD models.

3.3. The structure of anterior cingulate cortex pyramidal neurons is altered in 6-m 5×familial Alzheimer disease mice

Mutations in the genes for amyloid precursor protein and presenilins (PS1 and PS2) increase production of β-amyloid 42 ($A\beta_{42}$) and cause familial AD. The 5×FAD mice generate $A\beta_{42}$ almost exclusively and rapidly by coexpressing FAD mutant amyloid precursor protein and PS1.[56] Quantification of amyloid burden is identified by thioflavin S staining. We compared the Aβ area of 5×FAD mice and found it was increased significantly over time (**Figs. 4A and B**). The cholinergic and glutamatergic systems are traditionally regarded as the dominant contributors of excitatory or inhibitory imbalance and pathogenesis in the AD brain because of the glutamatergic and cholinergic neuronal excitability which was induced by Aβ aberrant accumulation.[8,59] To confirm the proportion of glutamatergic neurons in ACC, we accessed the Ca^{2+}/CaMKII$^+$ neurons by confocal scans and found no significant difference between 5×FAD and WT (**Figs. 4C and D**). Given this, we speculate that the Aβ42 altered the neuronal functions.

Alteration of excitatory synaptic function is the strongest correlation to the pathological disturbance of cognitive ability observed in the early stage of AD. In addition to reduce glutamatergic synaptic transmission and long-term potentiation, Aβ oligomers mediate the propagation of the synaptic pathology characterized by a decreased spine density of neighboring healthy neurons.[11] To figure out the variation of the neuronal structure, Golgi-Cox staining followed by dendritic reconstruction and spine morphology rebuilding was performed on tissue sections of the ACC (**Figs. 5A–E**). In view of the pathological alteration at the 6 m group is sufficient to cover the disease characteristics, the Golgi-Cox staining was applied across naïve and CFA-treated groups at 3-m and 6-m mice.

The complexity and dendritic length of ACC pyramidal neurons were reduced in 6-m 5×FAD mice (**Figs. 5F and G**) as well as the spine density and mature spine percentage (**Figs. 5H–J**). However, the alterations were not observed in 3-m 5×FAD mice. This difference between 3 m and 6 m mice correlates very well with behavioral and in vivo electrophysiological results, suggesting the pathogenic processes underlying AD may relate to the mechanical insensitivity after CFA injection. Thus, the deficiency

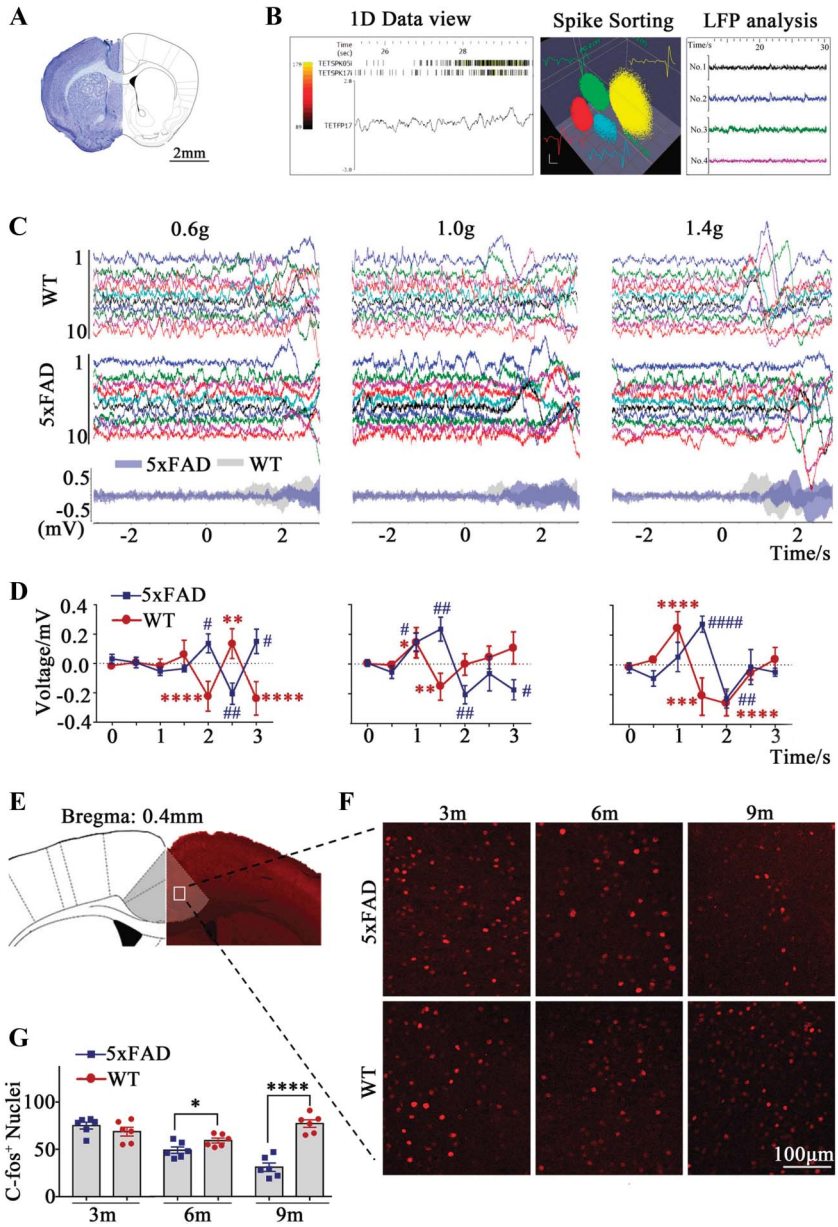

Figure 2. Attenuated complete Freund adjuvant–induced local field potential alteration and c-fos expression in ACC of 5×FAD mice. (A) Representative track of the tetrode electrode in the ACC brain region of mouse. Blue traces show the electrode array. Scale bar: 2 mm. (B) Representative images of spike offline sorting and LFP analysis. 1D viewer of LFP and action potential (left), 4 well-isolated units (cluster and waveforms) in the PCA plot recorded from a single tetrode (middle), and LFP over time from 4 adjacent channels (right). (C) LFP changes with different intensity filament stimulus. Each intensity stimulus (0.6, 1.0, and 1.4 g) is applied for 10 times (top), and the grey and blue areas represent the SEM voltage (bottom). (D) The amplitude values of voltages are compared with baseline every 500 ms after stimulus (WT: $^{*}P < 0.05$; $^{**}P < 0.01$; $^{***}P < 0.001$; $^{****}P < 0.0001$, 5×FAD: $\#P < 0.05$; $\#\#P < 0.01$; $\#\#\#\#P < 0.0001$, unpaired Student *t* test). (E) The schematic of ACC (grey shaded area) and the selected area analysed (white solid line). (F) Representative image of c-fos expression in ACC from each group. (G) Comparison of c-fos^{+} nuclei in ACC 4 hours after CFA injection between 5×FAD and WT group (n = 6 per group, $^{*}P < 0.05$ $^{****}P < 0.0001$; unpaired Student *t* test). ACC, anterior cingulate cortex; CFA, complete Freund adjuvant; FAD, familial Alzheimer disease; LFP, local field potential; WT, wild-type.

of neuronal activity is very likely associated with the alteration of the neuronal structure in ACC.

3.4. Genetic modulation of anterior cingulate cortex excitatory neurons altered the pain response

Optogenetics approach has been used to restore the excitability of glutamatergic neurons induced by deficiency of synaptic structural plasticity.[20] We manipulated the glutamatergic neurons in ACC that expressed ChR2 which linked to CaMKII promotor by adeno-associated virus (AAV) vector (**Fig. 6A**). The 450-nm laser stimulation was delivered at 0.1 Hz and lasted for 180 minutes after CFA injection (**Fig. 6B**). The units responsive to 1.4 g stimuli pre-CFA and 0.6 g stimuli post-CFA show significant increase during laser stimulation (**Fig. 6C**). Without genetic manipulation, the statistical difference exits between WT^{sham} and $5\times FAD^{sham}$ ($5\times FAD^{sham}$ vs WT^{sham}, **Fig. 6D**). As expected, the pain response of $5\times FAD^{ChR2}$ mice was rescued after the laser activation which the withdrawal rate elevated to the level of WT^{ChR2} or WT^{sham} ($5\times FAD^{ChR2}$ vs $WT^{ChR2\ or\ sham}$, **Fig. 6D**). There was no significant effect of laser stimulation on the paw withdrawal rate of WT animals (WT^{ChR2} vs WT^{sham}, **Fig. 6D**).

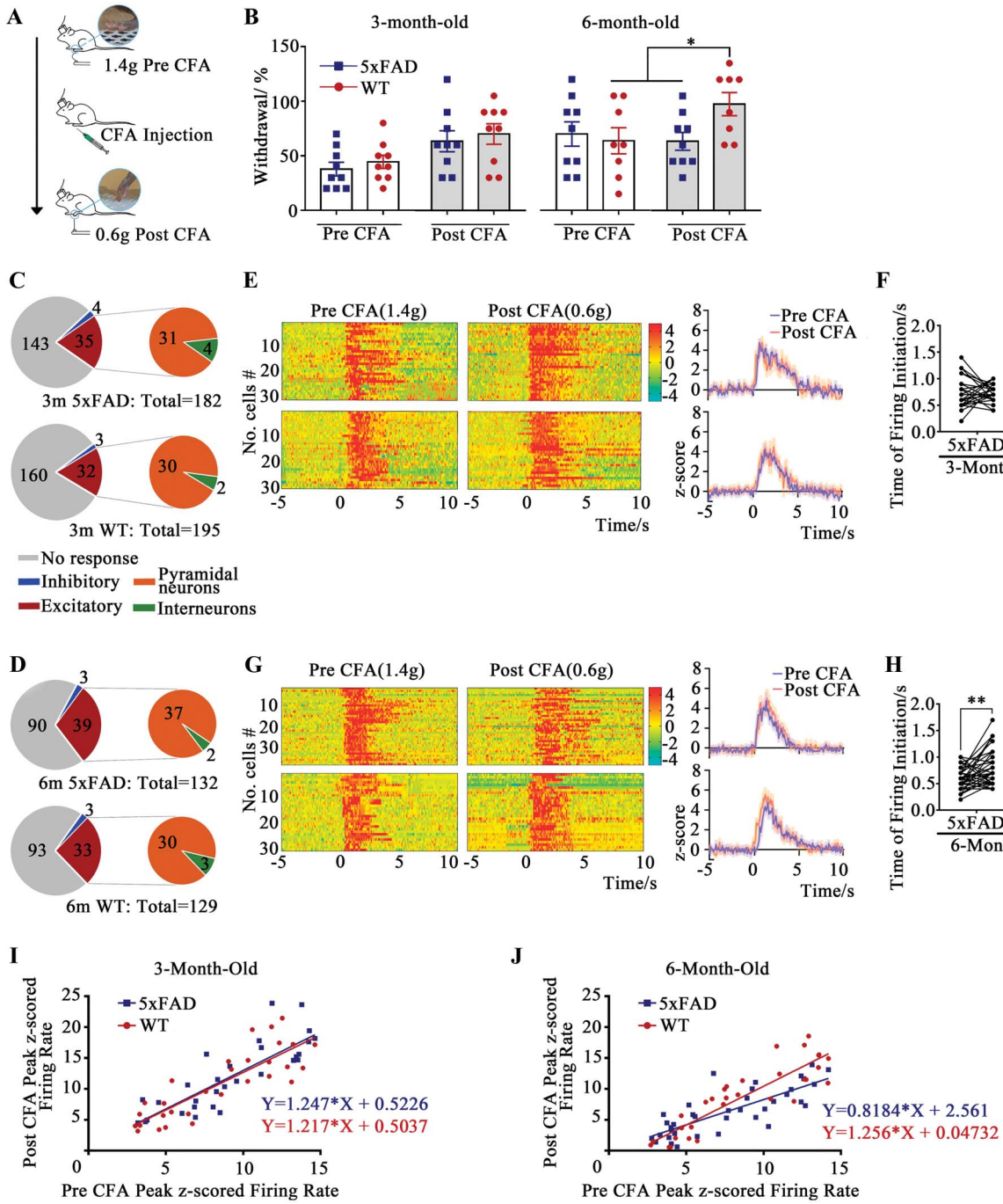

Figure 3. Delayed firing initiation and reduced peak z score in ACC putative pyramidal neurons of 6-m 5×FAD mice. (A) Schematic diagram of mechanical threshold measurement during the trial of in vivo electrophysiology recording. (B) The paw withdrawal percentage between 5×FAD and WT (3 m: both groups, n = 9; 6 m: 5×FAD, n = 9, WT, n = 8) (*$P < 0.05$, unpaired Student *t* test). (C and D) The number of responsive units including inhibitory and excitatory in total units recorded in ACC of 5×FAD (left top, 3 m: 182 units from 8 mice; 6 m: 132 units from 8 mice) and WT mice (left bottom, 3 m: 195 units from 8 mice; 6 m: 129 units from 8 mice). The numbers of putative pyramidal cells and putative interneurons in excitatory units (right top and bottom). (E) The firing heatmaps of the neurons at 3 m mice which responded to 1.4 g filament stimuli pre-CFA injection (5×FAD, left top; WT, left bottom) and 0.6 g stimuli post-CFA injection (5×FAD, middle top; WT, middle bottom). Plots to the right show the z score of responsive neurons (mean and SEM). (F) The comparison of firing initiation time between 1.4 g stimuli pre-CFA and 0.6 g stimuli post-CFA in the 5×FAD and WT mice (3 m). (G) Same as E at 6 m mice. (H) Same as F at 6 m mice. (**$P < 0.01$, paired Student *t* test). (I) A robust linear regression model was used to fit the peak z-scored firing rates and to calculate the slope of the linear regression line of all ACC neurons that demonstrated responsive to 0.6 g stimuli and 1.4 g stimuli (3-m 5×FAD mice: the equation is: $Y = 1.247 \times X + 0.5226$, $R^2 = 0.6909$, n = 31; 3-m WT mice: $Y = 1.217 \times X + 0.5037$, $R^2 = 0.5037$, n = 30). (J) Same as I. In the 6-m 5×FAD mice, the equation is: $Y = 0.8184 \times X + 2.561$, $R^2 = 0.6286$, n = 37. In the 6-m WT mice, the equation is: $Y = 1.256 \times X + 0.04732$, $R^2 = 0.7784$, n = 30. ACC, anterior cingulate cortex; CFA, complete Freund adjuvant; FAD, familial Alzheimer disease; WT, wild type.

To further assess the role of the ACC in modulation of inflammatory pain, we test whether inhibition of ACC glutamatergic neurons could decrease the withdrawal response to filament stimulus. The gene of human M4 muscarinic designer receptors exclusively activated by designer drugs receptor coupled to Gq (hM4D) was transfected to inhibit the excitatory neuronal activities. Clozapine-N-oxide, the

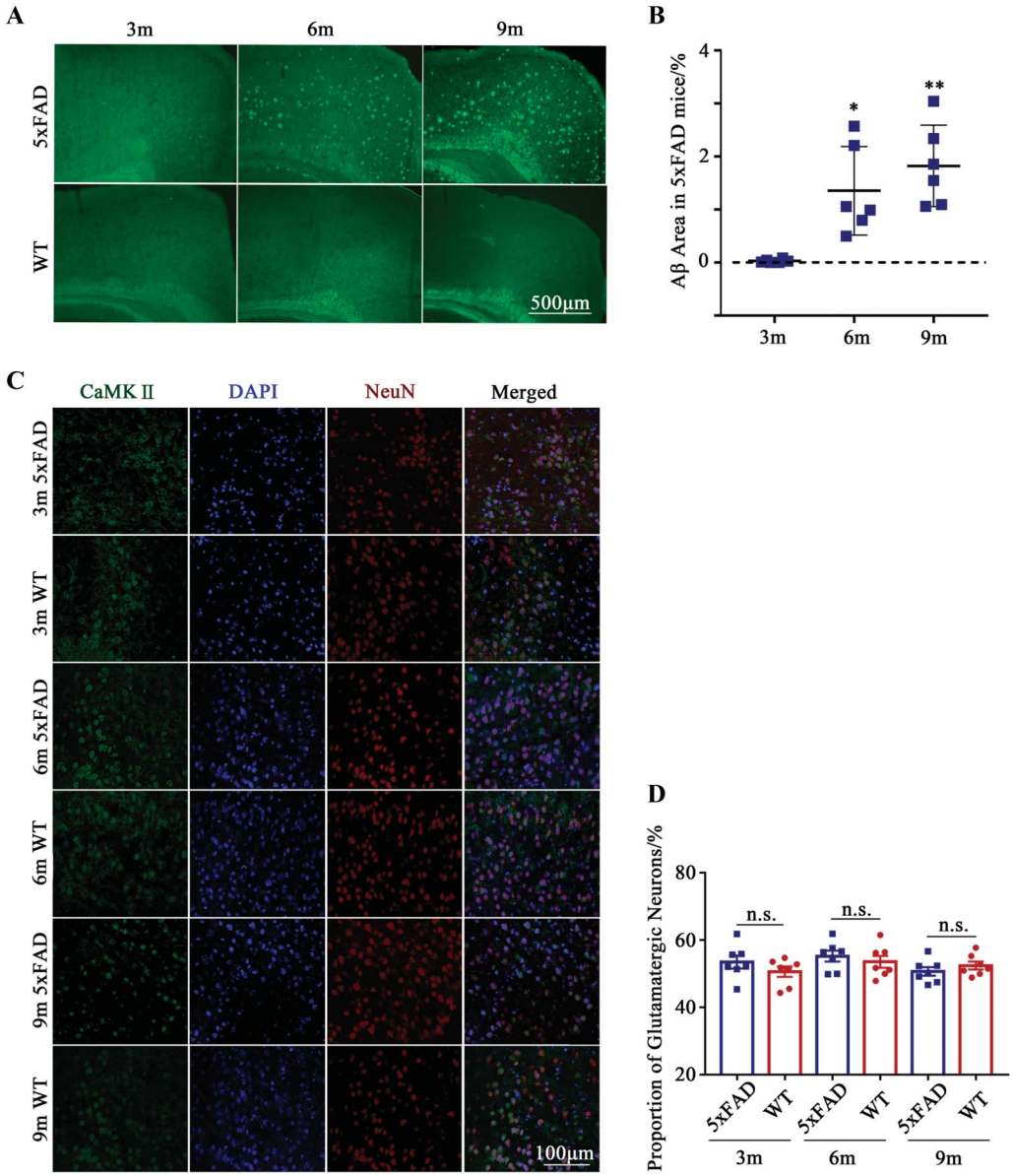

Figure 4. Identify the area of amyloid deposition and the proportion of glutamatergic neurons in ACC. (A) Representative fluorescence images of ThioS staining of 3, 6, 9-m 5×FAD and WT mice (scale bars, 500 μm). (B) Quantification of the percentage of the ThioS fluorescence area in 5×FAD mice (n = 6 for each group) (*$P < 0.05$, **$P < 0.01$, unpaired Student *t* test). (C) ACC neurons of 3, 6, 9-m 5×FAD and WT mice colabelled with CaMKIIα (green), DAPI (blue), and NeuN (red) are indicated by arrowheads (scale bars, 100 μm). (D) Proportions of glutamatergic neurons in the ACC of each group (n = 7 per group) ($P > 0.05$, unpaired Student *t* test). ACC, anterior cingulate cortex; WT, wild type.

selective activator of designer receptors exclusively activated by designer drugs, was intraperitoneal injected 1 hour before CFA injection (**Fig. 6E**). Not surprisingly, the neuronal activity was inhibited with 0.6 g stimulus after CFA (**Fig. 6F**). Under the inflammatory condition, the withdrawal percentage of WT^{hM4D} was significantly reduced (WT^{hM4D} vs WT^{sham}, **Fig. 6G**).

These genetic manipulations on ACC glutamatergic neurons regulate the limb withdrawal response, suggesting the crucial role of ACC in regulation of the inflammatory pain.

3.5. In vivo inhibition of Rac1 activity and actin polymerization decreases the pain threshold accompanied with dendritic spine reduction and neuronal inhibition

As we have demonstrated the consistency among decreased dendritic spine density, neuronal hypoexcitability, and mechanical hypesthesia in adult 5×FAD mice, we wonder whether the dendritic spine loss is the primary cause.

The Rho family of GTPases is believed to regulate various aspects in different biological systems.[49] The Rho-GTPases play well-defined roles in determining dendrite and dendritic spine development and morphology.[36,55] The Rac1 and RhoA, 2 members of Rho family, are involved in spine formation.[50,54] The Rac1 and F-actin regulation were disrupted in Alzheimer disease mice.[7,37] The inhibition of Rho kinase by its antagonist would reduce the morphing of spine head.[79] We use the Rac1-specific inhibitor NSC to disrupt the spine structure by blocking the guanine exchange factors. The inhibitor was intraventricularly injected twice a day for 3 days (**Fig. 7A** and Supplementary Fig. 4A, available at http://links.lww.com/PAIN/B618). The CFA injection and von Frey test were applied after the NSC delivery.

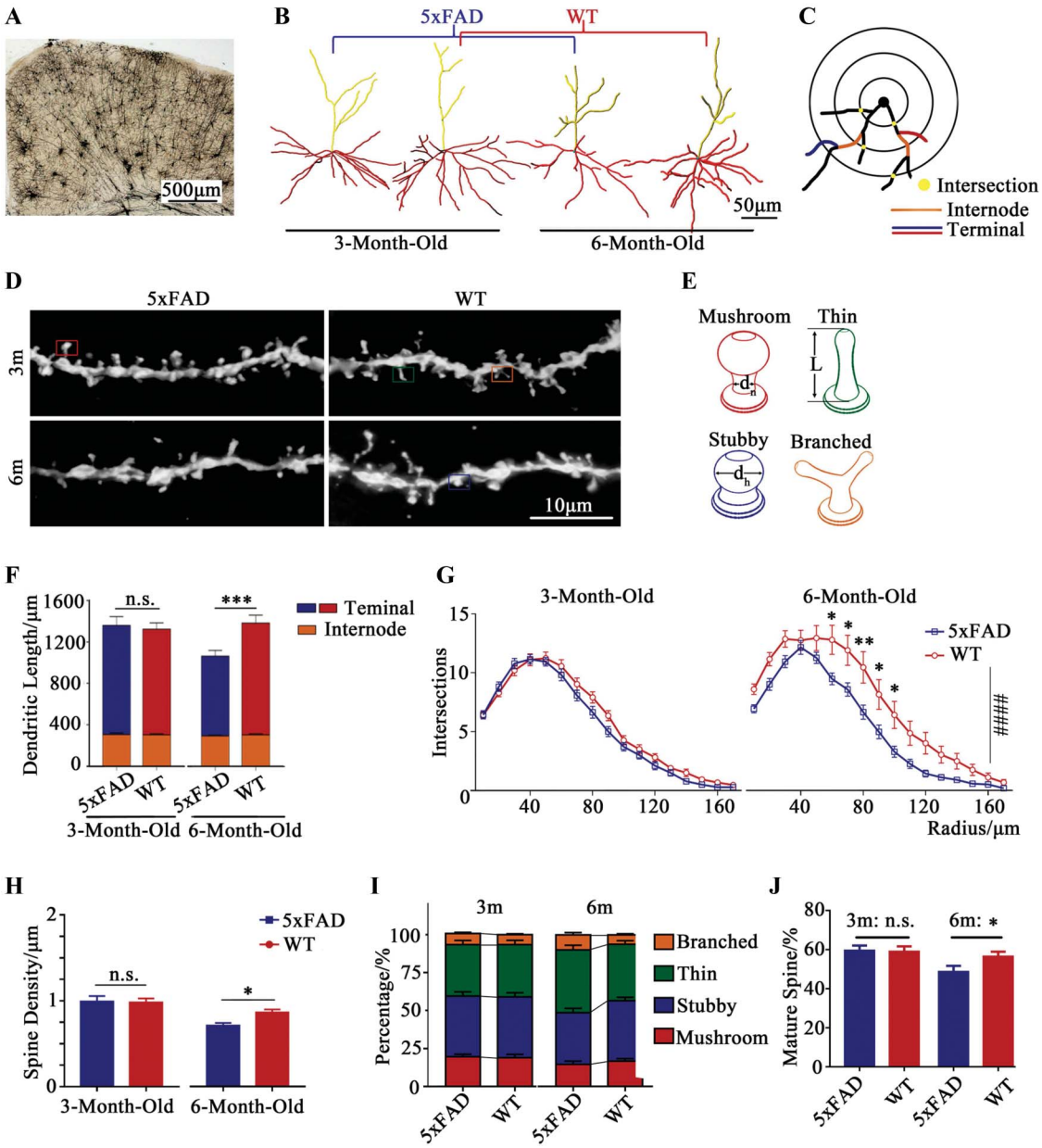

Figure 5. Structural alteration in anterior cingulate cortex pyramidal neurons of 6-m 5×FAD mice. (A) A representative micrograph of ACC with Golgi staining (scale bars, 500 μm). (B) Reconstructed ACC pyramidal neurons with Golgi staining. The basilar dendritic (red) is selected to analysis the complexity of dendrites (scale bars, 50 μm). (C) Schematic diagram of the method to calculate the number of intersections and dendritic length. The basilar dendritic profile and dendritic length of ACC pyramidal neurons are evaluated by using the concentric-ring method of Sholl. (D) Representative-inverted Golgi staining images show spines on basal dendrites in layer IV/V pyramidal neurons in ACC; the spines can be categorized as mushroom (red), stubby (blue), thin (green) and branched (orange) subtypes (scale bars, 10 μm). (E) Schematic diagram of the spine subtypes. (F) The basilar dendritic length of ACC pyramidal neurons: 3 m (5×FAD, 28 neurons from 5 mice; WT, 34 neurons from 5 mice) AND 6 m (5×FAD, 28 neurons from 5 mice; WT, 27 neurons from 5 mice) (***$P < 0.001$, unpaired Student *t* test). (G) Quantification the dendritic intersection of 5×FAD and WT mice at 3 and 6 m with sholl analysis (*$P < 0.05$, **$P < 0.01$, unpaired Student *t* test). Two-way ANOVA was performed to investigate the effects of genotype at 3 m and 6 m mice ($F(1, 901) = 75.74$, ####$P < 0.0001$). (H) Spine density of 5×FAD mice (35 dendrites from 3-m and 6-m mice, each n = 5) and WT mice (30 dendrites from 3 m and 6 m mice, each n = 5) *$P < 0.05$ unpaired Student *t* test). (I) Percentage of 4 spine subtypes in 5×FAD and WT mice. (J) The proportion of mature spines in 5×FAD and WT mice (*$P < 0.05$, unpaired Student *t* test). ACC, anterior cingulate cortex; ANOVA, analysis of variance; FAD, familial Alzheimer disease; WT, wild type.

The dendritic complexity shows no difference between WT + NSC and WT + saline (**Fig. 7B** top). Most 5×FAD dendrites show less complexity than WT (data table shows the statistics difference, **Fig. 7B** bottom). The same differences were found in dendritic length (**Fig. 7C**). Spine density was lowered in WT + NSC, whereas 5×FAD + saline showed the least density (**Fig. 7E**). The inhibition of Rho kinase does not change the percentage of different spine morphology and mature proportion in WT mice (no significant difference between WT + NSC and WT + saline, **Figs. 7F and G**). However, the 5×FAD shows different composition of spine morphology (**Fig. 7F**) and decreased mature proportion (**Fig. 7G**). Furthermore, the limb withdrawal rate decreases in the WT + NSC group 4 hours after CFA injection and returns to normal after 24 hours post-CFA (**Fig. 7H** and Supplementary Fig. 4B, available at http://links.lww.com/PAIN/B618). The delayed initiation of firing and the lowered peak

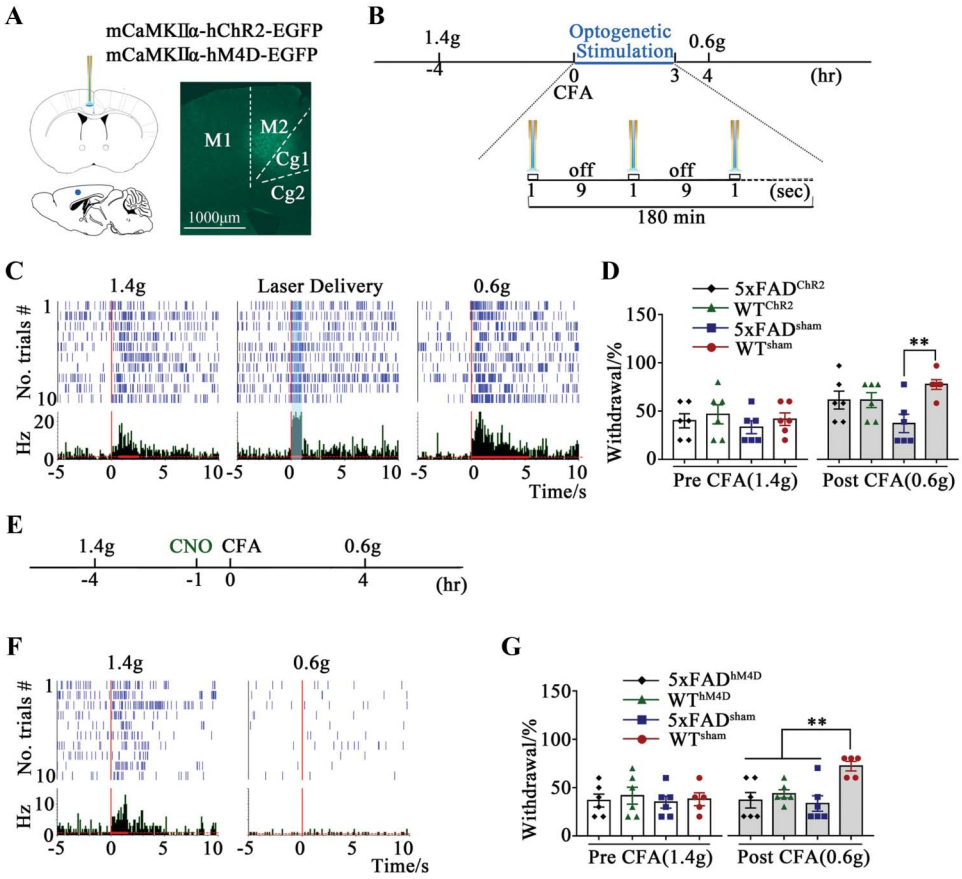

Figure 6. Activation and inhibition of anterior cingulate cortex glutamatergic neurons in von Frey tests. (A) Schematic and representative image of ChR2 or hM4D in 6-m 5×FAD and WT mice with an optical fiber in the ACC region. (B) Schematic of optogenetic modulation. First: 1.4 g filament stimuli 4 hours pre-CFA, next: 450-nm light stimulus chain (pulse: 0.1 Hz, 180 minutes), and last: 0.6 g filament stimuli 4 hours post-CFA. (C) Representative perievent rasters of the same unit with different stimulus in 6-m 5×FAD mice (left: 1.4 g stimuli pre-CFA, middle: laser stimuli, and right: 0.6 g stimuli post-CFA. (D) The paw withdrawal percentage before and after laser stimulation in all groups. No significant difference was found between $5\times FAD^{ChR2}$ and WT^{ChR2} or WT^{sham} (n = 6 in each group) (**$P < 0.01$, unpaired Student *t* test). (E) Schematic of chemogenetic modulation. First: 1.4 g filament stimuli 4 hours pre-CFA, next: CNO was injected intraperitoneally 1 hour pre-CFA, and last: 0.6 g filament stimuli 4 hours post-CFA. (F) Representative perievent rasters of the ACC neuron in 6-m 5×FAD mice (left: 1.4 g filament stimuli pre-CFA and right: 0.6 g filament stimuli post-CFA). (G) The paw withdrawal percentage with CNO inhibition in all groups. Significant difference was found between WT^{sham} and other 3 groups ($5\times FAD^{hM4D}$, $5\times FAD^{sham}$, and WT^{hM4D}: n = 6; WT^{sham}: n = 5) (**$P < 0.01$, unpaired Student *t* test). ACC, anterior cingulate cortex; CFA, complete Freund adjuvant; CNO, clozapine-N-oxide; FAD, familial Alzheimer disease; WT, wild type.

firing rate in neurons of WT + NSC indicate the inhibited neuronal activity (**Figs. 7I and J**).

The polymerization of F-actin could be inhibited while down-regulating the Rac1/PAK/LIMK/Cofilin signaling pathway.[80] Cytochalasin D, a widely used downstream inhibitor of actin polymerization, was chosen to further confirm the function of depolymerization. The results show the reduction of spine density and mature spine proportion (**Figs. 8A–D**). In addition, the pain response in WT + CD was weaker at 4 and 24 hours after CFA injection compared with WT + saline (**Fig. 8E** and Supplementary Fig. 4C, available at http://links.lww.com/PAIN/B618). Moreover, the neuronal firing initiation time was delayed, and the slope of linear fit was reduced in the WT + CD group (**Figs. 8F and G**).

4. Discussion

In this study, we sought to discover a bidirectional regulation of ACC excitatory neuronal activity and inflammatory mechanical pain response, which put forward a neural mechanism of hypesthesia in AD. Accumulating evidences have documented that the correlation between the changes of neuronal activity in ACC and several types of chronic pain.[22,39]

The LFP reflects the activities of population neurons and implies the dynamics of local network.[44] As the intensity of filament stimulus changes, so does the LFP amplitude. We managed to figure out that the c-Fos expression and post-CFA or pre-CFA peak z-score ratio is decreased in adult 5×FAD mice compared with controls. In addition, the initiation pattern of neuronal firing starts with a delay which implies the transmission inefficiency. These findings are inconsistent with the textbook-provided view that the "medial" pain system exclusively mediates the affective component of pain.[2] Animal studies about the function of the ACC in pain describe an exclusive role in pain-related negative affect but not in the sensory component of pain.[21,30,61] Pregenual ACC is the main relative area of nociception, whereas the cg1 of cingulate cortex is a cytoarchitecturally and functionally distinct subregion.[23,30,31,85] Then, we targeted on this specific brain region where the evoked field potential changes.

We speculate the mechanism under the hypesthesia of 5×FAD mice may be due to the deficiency of synaptic neurotransmission. Dendritic spines are the major sites of receiving the excitatory input, and their morphological specialization has been linked to synaptic plasticity.[28] The spine

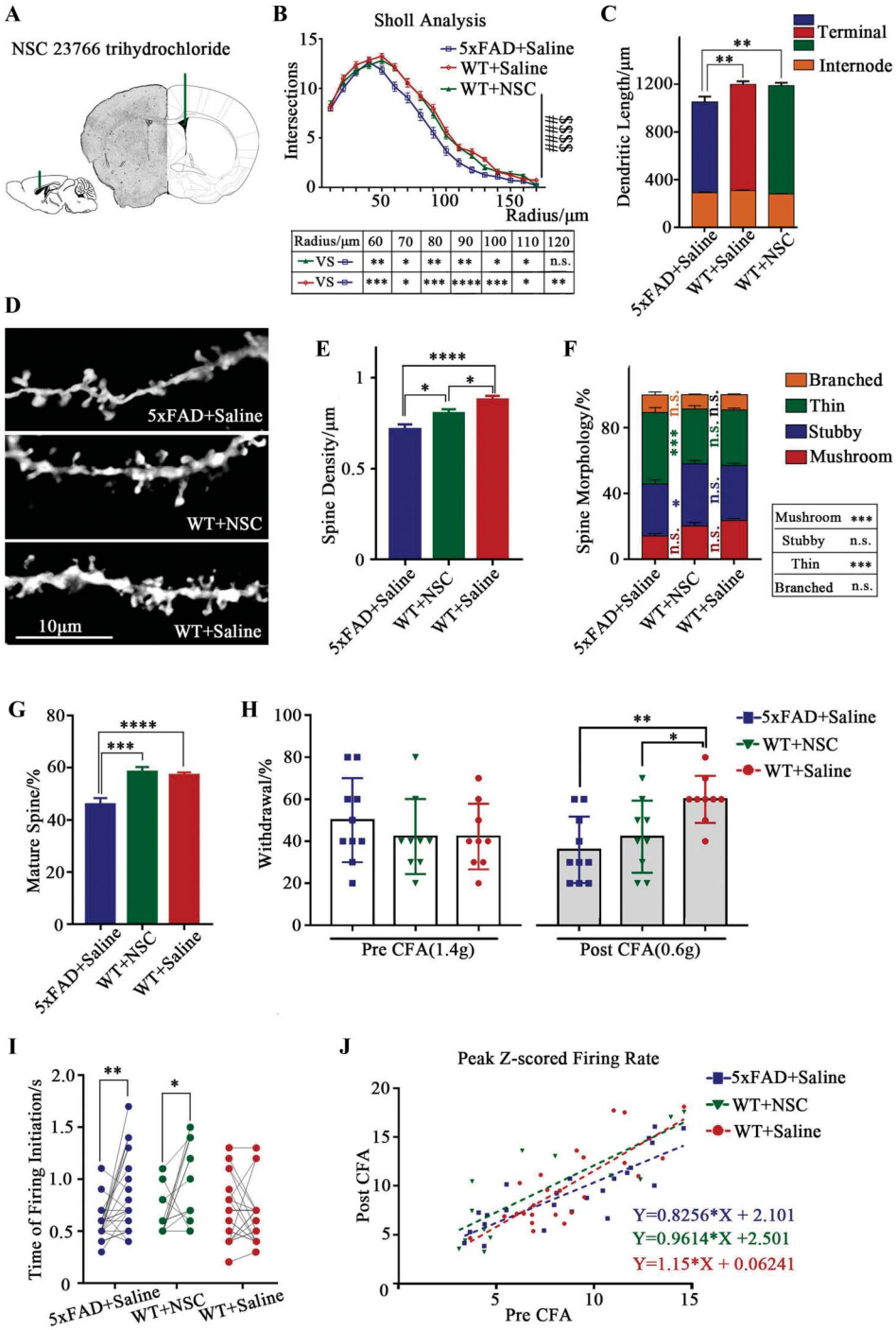

Figure 7. Reduced spine density which induced by intracerebroventricular (i.c.v.) injection of NSC would elevate the mechanical threshold of WT mice. (A) Schematic of i.c.v. injection of NSC. (B) The quantification of the dendritic intersections of 5×FAD + saline, WT + saline, and WT + NSC with sholl analysis (5×FAD + saline: 36 neurons from 5 mice, WT + NSC: 35 neurons from 5 mice, and WT + saline: 49 neurons from 6 mice). The table at the bottom displays a multiple-comparison results (*$P < 0.05$; **$P < 0.01$; ***$P < 0.001$; ****$P < 0.0001$, unpaired Student *t* test). Two-way ANOVA was performed to investigate the effects of NSC or saline (5×FAD + saline vs WT + saline: $F(1, 1377) = 106.2$, ####$P < 0.0001$) (5×FAD + saline vs WT + NSC: $F(1, 1139) = 65.62$, $$$$$P <$ 0.0001). (C) The basilar dendritic length of ACC pyramidal neurons is evaluated by the concentric-ring method of Sholl (**$P < 0.01$, unpaired Student *t* test). (D) Inverted Golgi staining of spines in basal dendrites of layer IV/V pyramidal neurons in ACC. (E) The spine density decreases significantly after NSC injection in WT mice (WT + NSC: 41 dendrites from 5 mice and WT + saline: 47 dendrites from 6 mice). The density of spine was reduced in 5×FAD + saline (35 dendrites from 5 mice) (*$P < 0.05$, ****$P < 0.0001$, unpaired Student *t* test). (F) Percentages of spine subtypes in ACC of 5×FAD + saline, WT + saline, and WT+ NSC mice. The table performs the comparison between 5×FAD + saline group and WT + saline (*$P < 0.05$, ***$P < 0.001$, unpaired Student *t* test). (G) Percentage of mature spines in 5×FAD + saline mice is significantly lower than WT + NSC or WT + saline (***$P < 0.001$, ****$P < 0.0001$, unpaired Student *t* test). (H) The paw withdrawal percentage of each group pre-CFA and post-CFA (5×FAD + saline: n = 10, WT + NSC: n = 9, and WT + saline: n = 9) (*$P < 0.05$, **$P < 0.01$, unpaired Student *t* test). (I) The initiations of neuronal firing between 1.4 g filament stimuli pre-CFA and 0.6 g filament post-CFA (5×FAD + saline: 24 neurons from 5 mice, WT + NSC: 13 neurons from 5 mice, and WT + saline: 24 neurons from 5 mice) (*$P < 0.05$, **$P < 0.01$, paired Student *t* test). (J) The linear regression line of all ACC neurons that demonstrated responsive to 1.4 g filament stimuli pre-CFA and 0.6 g filament stimuli post-CFA (5×FAD + saline: $R^2 = 0.6972$, n = 24; WT + NSC: $R^2 = 0.6719$, n = 13; WT + saline $R^2 = 0.6149$, n = 24). ACC, anterior cingulate cortex; ANOVA, analysis of variance; CFA, complete Freund adjuvant; FAD, familial Alzheimer disease; NSC, NSC23766 trihydrochloride; WT, wild type.

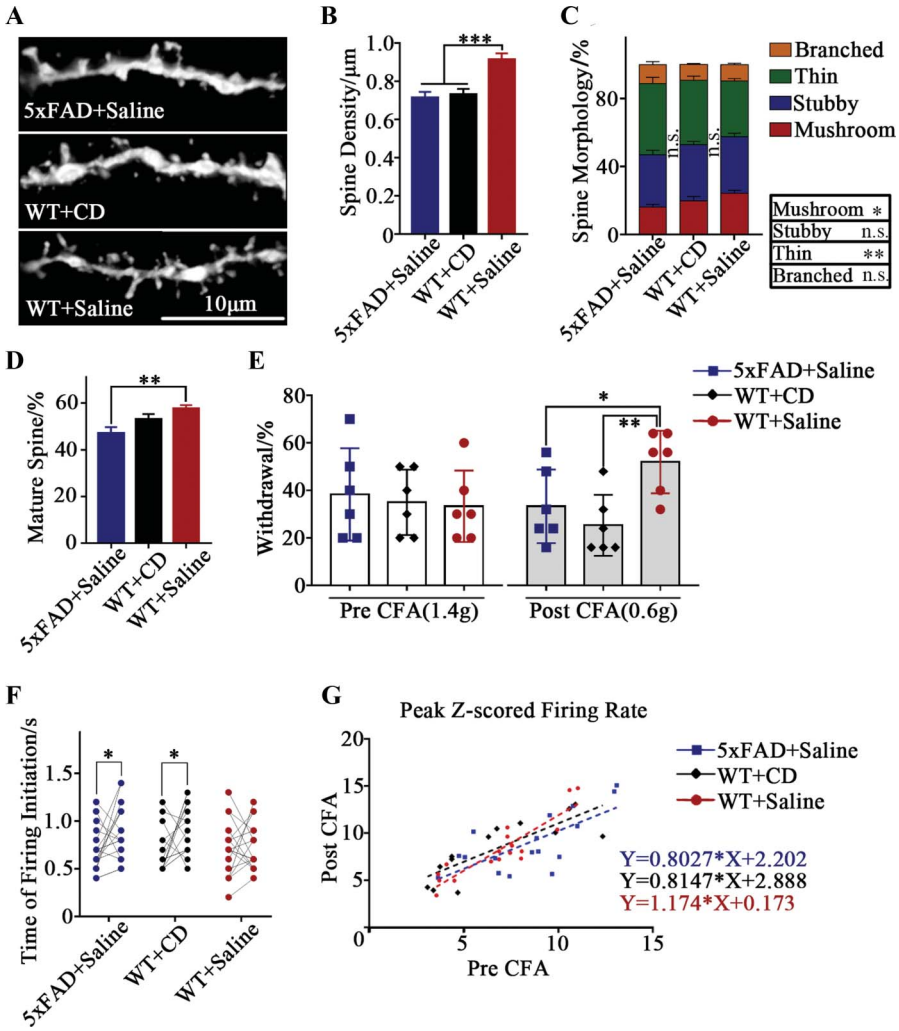

Figure 8. Reduced spine density which induced by i.c.v. injection of CD would elevate the mechanical threshold of WT mice. (A) Inverted Golgi staining of spines in basal dendrites of layer IV/V pyramidal neurons in ACC. (B) The spine density decreases significantly after CD injection in WT mice (25 dendrites from 5 mice in each group) (***$P < 0.001$, unpaired Student *t* test). (C) Percentages of spine subtypes of 5×FAD + saline, WT + saline, and WT+ CD groups. The table performs the comparison between 5×FAD + saline group and WT + saline (*$P < 0.05$, **$P < 0.01$, unpaired Student *t* test). (D) Percentages of mature spine of 5×FAD + saline, WT + CD, and WT + saline mice. The table performs the comparison between 5×FAD + saline group and WT + saline (**$P < 0.01$, unpaired Student *t* test). (E) The paw withdrawal percentages of each group pre-CFA and post-CFA (n = 6 in each group) (*$P < 0.05$, **$P < 0.01$, unpaired Student *t* test). (F) The initiations of neuronal firing between 1.4 g filament stimuli pre-CFA and 0.6 g filament stimuli post-CFA (5×FAD + saline: 17 neurons from 6 mice, WT + CD: 13 neurons from 6 mice, and WT + saline: 17 neurons from 6 mice) (*$P < 0.05$, paired Student *t* test). (G) The linear regression line of all ACC neurons that demonstrated responsive to 1.4 g filament stimuli pre-CFA and 0.6 g filament stimuli post-CFA (5×FAD + saline: $R^2 = 0.5127$, n = 17; WT + CD: $R^2 = 0.6767$, n = 13; WT + saline $R^2 = 0.8098$, n = 17). ACC, anterior cingulate cortex; CD, cytochalasin D; CFA, complete Freund adjuvant; FAD, familial Alzheimer disease; WT, wild type.

remodeling is proposed as both a cause and a consequence of chronic pain.[68,73,75] In both animal models and clinical trials of patients with AD, changes in dendritic spines dynamics which triggered by M1 microglia activation, amyloid burden, or tau hyperphosphorylation are proved by studies using multiple technologies.[4,7,51,91] The overall proportions of glutamatergic neurons remain unchanged in 6 and 9-m 5×FAD mice, and then, we try to investigate the alteration of the dendritic structure. In consistent with the comparative result of neuronal activity, the result is similar between experimental and control groups in 3-m old in 2 aspects: dendritic complexity and spine density. These results suggest the deficiency of glutamatergic transmission in ACC of AD subjects mediate the alteration of neuronal activity and eventually influence the nociceptive response which is consistent with previous studies.[24,47] Modulation of the morphology or density of dendritic spines contributes to the changes of synaptic plasticity which is believed to mediate the long-term memory.[14] Chronic pain can be seen as the persistent sensory memory and inability to extinguish the painful memory, whereas the LTP/LTD in the dorsal horn of the spinal cord and cingulate cortex is demonstrated causally related to chronic pain.[6,64,97] Dendritic spines contain postsynaptic density, several kinds of functional proteins, actin, actin binding, and actin regulatory proteins controlled by upstream molecules such as small GTPase.[12,14,16] The infusion of Rac1 GTPase inhibitor NSC before fear conditioning or neuropathic pain blocks both the processes of memory storage and hyperalgesia.[43,76] Thus, we wonder the alterations of spine density as well as neuronal activity and behavioural result in WT mice after i.c.v. administration of NSC. The NSC application significantly decreases the spine density and occurrence of withdrawal response after CFA injection. Neurons under the Rac1 GTPase inhibitory condition show a weaker response, as indicated by a decrease in the slope of linear fit and a significant delay of firing initiation. Acting as a

downstream F-actin remodeling inhibitor, CD functioned in modulation of pain response and neuronal activity as well. These modulations of spine density could induce similar behavioural results in AD models.

CaMKII is known to play a key role in synaptic plasticity.[5,52] The repetitive optogenetic activation of CaMKII$^+$ neurons caused enhancement of optogenetically evoked firing of local coactivated neurons.[95] By using the optogenetics and chemogenetics manipulations to target specific cell population, we observe that the inflammation-induced mechanical hypersensitivity is tightly linked and regulated by ACC. The optogenetic activation of the glutamatergic neurons decrease the withdrawal threshold in 5×FAD mice, whereas the chemogenetics elevates the pain threshold in WT mice, suggesting the glutamatergic neurons in ACC play a crucial role in pain processing of inflammatory pain. Owing to the synaptic proteins upregulation and spine density increase that occur 24 hours after stimulation, we speculate that the enhanced neuronal excitability plays a major part in behavioral changes.[46]

This study illustrates the relationships among pain response, neuronal activity, and dendritic spine. Our behavioral tests reveal that the 5×FAD mice develop a hypesthesia from 3 m to over 6 m old. Electrical neurophysiology in vivo recording demonstrates the relevance of ACC neural activity to pain response. Then, the result is further verified by genetic manipulations. Imaging pinpoints the dendritic spine deficiency in ACC neurons of 5×FAD mice and is likely related to the alteration of pain response, which can be mimicked by WT mice with inhibition of the formation of the dendritic spine. Taken together, the alteration of pain processing in AD modeling mice could be the linked to dendritic spine loss in ACC pyramidal neurons. Owing to chronic pain is underdiagnosis and undertreatment in patients with AD, the nonverbal assessment which contains facial expression, electrophysiological examination, detection of biomarker, and so on is needed.[25]

Conflict of interest statement

The authors have no conflicts of interest to declare.

Acknowledgements

This work was supported by the Chinese National Natural Science Foundation of China (Grant numbers 62127810, 31701217, and 81970418), Shanghai Key Laboratory of Health Identification and Assessment (21DZ2271000).

Appendix A. Supplemental digital content

Supplemental digital content associated with this article can be found online at http://links.lww.com/PAIN/B618.

Article history:
Received 3 November 2021
Received in revised form 25 March 2022
Accepted 28 March 2022
Available online 16 April 2022

References

[1] Allman JM, Hakeem A, Erwin JM, Nimchinsky E, Hof P. The anterior cingulate cortex. The evolution of an interface between emotion and cognition. Ann N Y Acad Sci 2001;935:107–17.
[2] Alvarez VA, Sabatini BL. Anatomical and physiological plasticity of dendritic spines. Annu Rev Neurosci 2007;30:79–97.
[3] Aman Y, Pitcher T, Simeoli R, Ballard C, Malcangio M. Reduced thermal sensitivity and increased opioidergic tone in the TASTPM mouse model of Alzheimer's disease. PAIN 2016;157:2285–96.
[4] Andrew RJ, Fernandez CG, Stanley M, Jiang H, Nguyen P, Rice RC, Buggia-Prevot V, De Rossi P, Vetrivel KS, Lamb R, Argemi A, Allaert ES, Rathbun EM, Krause SV, Wagner SL, Parent AT, Holtzman DM, Thinakaran G. Lack of BACE1 S-palmitoylation reduces amyloid burden and mitigates memory deficits in transgenic mouse models of Alzheimer's disease. Proc Natl Acad Sci U S A 2017;114:E9665–74.
[5] Ben-Simon Y, Rodenas-Ruano A, Alvina K, Lam AD, Stuenkel EL, Castillo PE, Ashery U. A combined optogenetic-knockdown strategy reveals a major role of tomosyn in mossy fiber synaptic plasticity. Cell Rep 2015;12:396–404.
[6] Bliss TV, Collingridge GL, Kaang BK, Zhuo M. Synaptic plasticity in the anterior cingulate cortex in acute and chronic pain. Nat Rev Neurosci 2016;17:485–96.
[7] Borin M, Saraceno C, Catania M, Lorenzetto E, Pontelli V, Paterlini A, Fostinelli S, Avesani A, Di Fede G, Zanusso G, Benussi L, Binetti G, Zorzan S, Ghidoni R, Buffelli M, Bolognin S. Rac1 activation links tau hyperphosphorylation and Abeta dysmetabolism in Alzheimer's disease. Acta Neuropathol Commun 2018;6:61.
[8] Bouteiller JC, Mergenthal AR, Hu E, Berger TW. Pathogenic processes underlying Alzheimer's disease: modeling the effects of amyloid beta on synaptic transmission. Conf Proc IEEE Eng Med Biol Soc 2019;2019: 1956–9.
[9] Bullock L, Bedson J, Chen Y, Chew-Graham CA, Campbell P. Comparative differences in musculoskeletal pain consultation and analgesic prescription for people with dementia: a UK-wide matched cohort study. PAIN 2021;162:2613–20.
[10] Burston JJ, Valdes AM, Woodhams SG, Mapp PI, Stocks J, Watson DJG, Gowler PRW, Xu L, Sagar DR, Fernandes G, Frowd N, Marshall L, Zhang W, Doherty M, Walsh DA, Chapman V. The impact of anxiety on chronic musculoskeletal pain and the role of astrocyte activation. PAIN 2019;160: 658–69.
[11] Caccavano A, Bozzelli PL, Forcelli PA, Pak DTS, Wu JY, Conant K, Vicini S. Inhibitory parvalbumin basket cell activity is selectively reduced during hippocampal sharp wave ripples in a mouse model of familial Alzheimer's disease. J Neurosci 2020;40:5116–36.
[12] Chazeau A, Mehidi A, Nair D, Gautier JJ, Leduc C, Chamma I, Kage F, Kechkar A, Thoumine O, Rottner K, Choquet D, Gautreau A, Sibarita JB, Giannone G. Nanoscale segregation of actin nucleation and elongation factors determines dendritic spine protrusion. EMBO J 2014;33:2745–64.
[13] Cole LJ, Farrell MJ, Duff EP, Barber JB, Egan GF, Gibson SJ. Pain sensitivity and fMRI pain-related brain activity in Alzheimer's disease. Brain 2006;129:2957–65.
[14] Costa JF, Dines M, Lamprecht R. The role of rac GTPase in dendritic spine morphogenesis and memory. Front Synaptic Neurosci 2020;12:12.
[15] de Waal MWM, van Dalen-Kok AH, de Vet HCW, Gimenez-Llort L, Konstantinovic L, de Tommaso M, Fischer T, Lukas A, Kunz M, Lautenbacher S, Lobbezoo F, McGuire BE, van der Steen JT, Achterberg WP. Observational pain assessment in older persons with dementia in four countries: observer agreement of items and factor structure of the Pain Assessment in Impaired Cognition. Eur J Pain 2020; 24:279–96.
[16] Duman JG, Mulherkar S, Tu YK, Cheng JX, Tolias KF. Mechanisms for spatiotemporal regulation of Rho-GTPase signaling at synapses. Neurosci Lett 2015;601:4–10.
[17] Etkin A, Egner T, Kalisch R. Emotional processing in anterior cingulate and medial prefrontal cortex. Trends Cogn Sci 2011;15:85–93.
[18] Fallon N, Chiu Y, Nurmikko T, Stancak A. Functional connectivity with the default mode network is altered in fibromyalgia patients. PLoS One 2016; 11:e0159198.
[19] Fan Z, Wu Y, Shen J, Ji T, Zhan R. Schizophrenia and the risk of cardiovascular diseases: a meta-analysis of thirteen cohort studies. J Psychiatr Res 2013;47:1549–56.
[20] Fieblinger T, Graves SM, Sebel LE, Alcacer C, Plotkin JL, Gertler TS, Chan CS, Heiman M, Greengard P, Cenci MA, Surmeier DJ. Cell type-specific plasticity of striatal projection neurons in parkinsonism and L-DOPA-induced dyskinesia. Nat Commun 2014;5:5316.
[21] Gao YJ, Ren WH, Zhang YQ, Zhao ZQ. Contributions of the anterior cingulate cortex and amygdala to pain- and fear-conditioned place avoidance in rats. PAIN 2004;110:343–53.
[22] Glass JM, Williams DA, Fernandez-Sanchez ML, Kairys A, Barjola P, Heitzeg MM, Clauw DJ, Schmidt-Wilcke T. Executive function in chronic pain patients and healthy controls: different cortical activation during response inhibition in fibromyalgia. J Pain 2011;12:1219–29.
[23] Gu L, Uhelski ML, Anand S, Romero-Ortega M, Kim YT, Fuchs PN, Mohanty SK. Pain inhibition by optogenetic activation of specific anterior cingulate cortical neurons. PLoS One 2015;10:e0117746.

[24] Hadjistavropoulos T, Herr K, Prkachin KM, Craig KD, Gibson SJ, Lukas A, Smith JH. Pain assessment in elderly adults with dementia. Lancet Neurol 2014;13:1216–27.
[25] Hamina A, Taipale H, Tanskanen A, Tolppanen AM, Karttunen N, Pylkkanen L, Tiihonen J, Hartikainen S. Long-term use of opioids for nonmalignant pain among community-dwelling persons with and without Alzheimer disease in Finland: a nationwide register-based study. PAIN 2017;158:252–60.
[26] Harris KM, Jensen FE, Tsao B. Three-dimensional structure of dendritic spines and synapses in rat hippocampus (CA1) at postnatal day 15 and adult ages: implications for the maturation of synaptic physiology and long-term potentiation. J Neurosci 1992;12:2685–705.
[27] Harris KM, Weinberg RJ. Ultrastructure of synapses in the mammalian brain. Cold Spring Harbor Perspect Biol 2012;4:a005587.
[28] Hering H, Sheng M. Dendritic spines: structure, dynamics and regulation. Nat Rev Neurosci 2001;2:880–8.
[29] Holtmaat A, Svoboda K. Experience-dependent structural synaptic plasticity in the mammalian brain. Nat Rev Neurosci 2009;10:647–58.
[30] Johansen JP, Fields HL. Glutamatergic activation of anterior cingulate cortex produces an aversive teaching signal. Nat Neurosci 2004;7: 398–403.
[31] Johansen JP, Fields HL, Manning BH. The affective component of pain in rodents: direct evidence for a contribution of the anterior cingulate cortex. Proc Natl Acad Sci U S A 2001;98:8077–82.
[32] John A, Reddy PH. Synaptic basis of Alzheimer's disease: focus on synaptic amyloid beta, P-tau and mitochondria. Ageing Res Rev 2021;65: 101208.
[33] Kameda T, Kaneuchi Y, Sekiguchi M, Konno SI. Measurement of mechanical withdrawal thresholds and gait analysis using the CatWalk method in a nucleus pulposus-applied rodent model. J Exp Orthop 2017; 4:31.
[34] Kang SJ, Kwak C, Lee J, Sim SE, Shim J, Choi T, Collingridge GL, Zhuo M, Kaang BK. Bidirectional modulation of hyperalgesia via the specific control of excitatory and inhibitory neuronal activity in the ACC. Mol Brain 2015;8:81.
[35] Koga K, Li X, Chen T, Steenland HW, Descalzi G, Zhuo M. In vivo whole-cell patch-clamp recording of sensory synaptic responses of cingulate pyramidal neurons to noxious mechanical stimuli in adult mice. Mol Pain 2010;6:62.
[36] Koleske AJ. Molecular mechanisms of dendrite stability. Nat Rev Neurosci 2013;14:536–50.
[37] Kommaddi RP, Das D, Karunakaran S, Nanguneri S, Bapat D, Ray A, Shaw E, Bennett DA, Nair D, Ravindranath V. Abeta mediates F-actin disassembly in dendritic spines leading to cognitive deficits in Alzheimer's disease. J Neurosci 2018;38:1085–99.
[38] Kragel PA, Kano M, Van Oudenhove L, Ly HG, Dupont P, Rubio A, Delon-Martin C, Bonaz BL, Manuck SB, Gianaros PJ, Ceko M, Reynolds Losin EA, Woo CW, Nichols TE, Wager TD. Generalizable representations of pain, cognitive control, and negative emotion in medial frontal cortex. Nat Neurosci 2018;21:283–9.
[39] Kulkarni B, Bentley DE, Elliott R, Julyan PJ, Boger E, Watson A, Boyle Y, El-Deredy W, Jones AK. Arthritic pain is processed in brain areas concerned with emotions and fear. Arthritis Rheum 2007;56:1345–54.
[40] Lee ZF, Huang TH, Chen SP, Cheng IH. Altered nociception in Alzheimer disease is associated with striatal-enriched protein tyrosine phosphatase signaling. PAIN 2021;162:1669–80.
[41] Li XY, Wang N, Wang YJ, Zuo ZX, Koga K, Luo F, Zhuo M. Long-term temporal imprecision of information coding in the anterior cingulate cortex of mice with peripheral inflammation or nerve injury. J Neurosci 2014;34: 10675–87.
[42] Li YD, Ge J, Luo YJ, Xu W, Wang J, Lazarus M, Hong ZY, Qu WM, Huang ZL. High cortical delta power correlates with aggravated allodynia by activating anterior cingulate cortex GABAergic neurons in neuropathic pain mice. PAIN 2020;161:288–99.
[43] Liao Z, Tao Y, Guo X, Cheng D, Wang F, Liu X, Ma L. Fear conditioning downregulates Rac1 activity in the basolateral amygdala astrocytes to facilitate the formation of fear memory. Front Mol Neurosci 2017;10:396.
[44] Linden H, Tetzlaff T, Potjans TC, Pettersen KH, Grun S, Diesmann M, Einevoll GT. Modeling the spatial reach of the LFP. Neuron 2011;72: 859–72.
[45] Liu JYW, Leung DYP. Pain treatments for nursing home residents with advanced dementia and substantial impaired communication: a cross-sectional analysis at baseline of a cluster randomized controlled trial. Pain Med 2017;18:1649–57.
[46] Lu H, Gallinaro JV, Normann C, Rotter S, Yalcin I. Time course of homeostatic structural plasticity in response to optogenetic stimulation in mouse anterior cingulate cortex. Cereb Cortex 2022;32:1574–92.
[47] Lukas A, Hagg-Grun U, Mayer B, Fischer T, Schuler M. Pain assessment in advanced dementia. Validity of the German PAINAD-a prospective double-blind randomised placebo-controlled trial. PAIN 2019;160: 742–53.
[48] Lukas A, Schuler M, Fischer TW, Gibson SJ, Savvas SM, Nikolaus T, Denkinger M. Pain and dementia: a diagnostic challenge. Z Gerontol Geriatr 2012;45:45–9.
[49] Luo L. Actin cytoskeleton regulation in neuronal morphogenesis and structural plasticity. Annu Rev Cel Dev Biol 2002;18:601–35.
[50] Luo L, Hensch TK, Ackerman L, Barbel S, Jan LY, Jan YN. Differential effects of the Rac GTPase on Purkinje cell axons and dendritic trunks and spines. Nature 1996;379:837–40.
[51] Montero-Crespo M, Dominguez-Alvaro M, Alonso-Nanclares L, DeFelipe J, Blazquez-Llorca L. Three-dimensional analysis of synaptic organization in the hippocampal CA1 field in Alzheimer's disease. Elife 2020;9: e57013.
[52] Murakoshi H, Shin ME, Parra-Bueno P, Szatmari EM, Shibata ACE, Yasuda R. Kinetics of endogenous CaMKII required for synaptic plasticity revealed by optogenetic kinase inhibitor. Neuron 2017;94:37–47.e35.
[53] Murakoshi H, Yasuda R. Postsynaptic signaling during plasticity of dendritic spines. Trends Neurosci 2012;35:135–43.
[54] Nakayama AY, Harms MB, Luo L. Small GTPases Rac and Rho in the maintenance of dendritic spines and branches in hippocampal pyramidal neurons. J Neurosci 2000;20:5329–38.
[55] Newey SE, Velamoor V, Govek EE, Van Aelst L. Rho GTPases, dendritic structure, and mental retardation. J Neurobiol 2005;64:58–74.
[56] Nuti R, Martini G, Merlotti D, De Paola V, Valleggi F, Gennari L. Bone metabolism in men: role of aromatase activity. J Endocrinol Invest 2007; 30:18–23.
[57] Oakley H, Cole SL, Logan S, Maus E, Shao P, Craft J, Guillozet-Bongaarts A, Ohno M, Disterhoft J, Van Eldik L, Berry R, Vassar R. Intraneuronal beta-amyloid aggregates, neurodegeneration, and neuron loss in transgenic mice with five familial Alzheimer's disease mutations: potential factors in amyloid plaque formation. J Neurosci 2006;26: 10129–40.
[58] Okamura K, Tanaka H, Yagita Y, Saeki Y, Taguchi A, Hiraoka Y, Zeng LH, Colman DR, Miki N. Cadherin activity is required for activity-induced spine remodeling. J Cell Biol 2004;167:961–72.
[59] Palop JJ, Mucke L. Amyloid-beta-induced neuronal dysfunction in Alzheimer's disease: from synapses toward neural networks. Nat Neurosci 2010;13:812–18.
[60] Penzes P, Cahill ME, Jones KA, VanLeeuwen JE, Woolfrey KM. Dendritic spine pathology in neuropsychiatric disorders. Nat Neurosci 2011;14: 285–93.
[61] Qu C, King T, Okun A, Lai J, Fields HL, Porreca F. Lesion of the rostral anterior cingulate cortex eliminates the aversiveness of spontaneous neuropathic pain following partial or complete axotomy. PAIN 2011;152: 1641–8.
[62] Rezaei S, Moturu A, Zhao S, Prkachin KM, Hadjistavropoulos T, Taati B. Unobtrusive pain monitoring in older adults with dementia using pairwise and contrastive training. IEEE J Biomed Health Inform 2021;25:1450–62.
[63] Rushworth MF, Behrens TE, Rudebeck PH, Walton ME. Contrasting roles for cingulate and orbitofrontal cortex in decisions and social behaviour. Trends Cognitive Sciences 2007;11:168–76.
[64] Sandkuhler J. Understanding LTP in pain pathways. Mol Pain 2007;3:9.
[65] Segal M. Dendritic spines and long-term plasticity. Nat Rev Neurosci 2005;6:277–84.
[66] Shankar GM, Li S, Mehta TH, Garcia-Munoz A, Shepardson NE, Smith I, Brett FM, Farrell MA, Rowan MJ, Lemere CA, Regan CM, Walsh DM, Sabatini BL, Selkoe DJ. Amyloid-beta protein dimers isolated directly from Alzheimer's brains impair synaptic plasticity and memory. Nat Med 2008;14:837–42.
[67] Sheng M, Sabatini BL, Sudhof TC. Synapses and Alzheimer's disease. Cold Spring Harbor Perspect Biol 2012;4:a005777.
[68] Simonetti M, Kuner R. Spinal Wnt5a plays a key role in spinal dendritic spine remodeling in neuropathic and inflammatory pain models and in the proalgesic effects of peripheral Wnt3a. J Neurosci 2020;40:6664–77.
[69] Smith DL, Pozueta J, Gong B, Arancio O, Shelanski M. Reversal of long-term dendritic spine alterations in Alzheimer disease models. Proc Natl Acad Sci U S A 2009;106:16877–82.
[70] Song D, Wang D, Yang Q, Yan T, Wang Z, Yan Y, Zhao J, Xie Z, Liu Y, Ke Z, Qazi TJ, Li Y, Wu Y, Shi Q, Lang Y, Zhang H, Huang T, Wang C, Quan Z, Qing H. The lateralization of left hippocampal CA3 during the retrieval of spatial working memory. Nat Commun 2020;11:2901.
[71] Stubbs B, Gaughran F, Mitchell AJ, De Hert M, Farmer R, Soundy A, Rosenbaum S, Vancampfort D. Schizophrenia and the risk of fractures: a systematic review and comparative meta-analysis. Gen Hosp Psychiatry 2015;37:126–33.

[72] Tada T, Sheng M. Molecular mechanisms of dendritic spine morphogenesis. Curr Opin Neurobiol 2006;16:95–101.
[73] Tan AM, Chang YW, Zhao P, Hains BC, Waxman SG. Rac1-regulated dendritic spine remodeling contributes to neuropathic pain after peripheral nerve injury. Exp Neurol 2011;232:222–33.
[74] Tan AM, Samad OA, Liu S, Bandaru S, Zhao P, Waxman SG. Burn injury-induced mechanical allodynia is maintained by Rac1-regulated dendritic spine dysgenesis. Exp Neurol 2013;248:509–19.
[75] Tan AM, Stamboulian S, Chang YW, Zhao P, Hains AB, Waxman SG, Hains BC. Neuropathic pain memory is maintained by Rac1-regulated dendritic spine remodeling after spinal cord injury. J Neurosci 2008;28: 13173–83.
[76] Tan AM, Waxman SG. Dendritic spine dysgenesis in neuropathic pain. Neurosci Lett 2015;601:54–60.
[77] Tan LL, Oswald MJ, Heinl C, Retana Romero OA, Kaushalya SK, Monyer H, Kuner R. Gamma oscillations in somatosensory cortex recruit prefrontal and descending serotonergic pathways in aversion and nociception. Nat Commun 2019;10:983.
[78] Tan LL, Oswald MJ, Kuner R. Neurobiology of brain oscillations in acute and chronic pain. Trends Neurosci 2021;44:629–42.
[79] Tashiro A, Yuste R. Regulation of dendritic spine motility and stability by Rac1 and Rho kinase: evidence for two forms of spine motility. Mol Cell Neurosci 2004;26:429–40.
[80] Tejada-Simon MV. Modulation of actin dynamics by Rac1 to target cognitive function. J Neurochem 2015;133:767–79.
[81] Urban R, Scherrer G, Goulding EH, Tecott LH, Basbaum AI. Behavioral indices of ongoing pain are largely unchanged in male mice with tissue or nerve injury-induced mechanical hypersensitivity. PAIN 2011;152: 990–1000.
[82] van Dam PH, Achterberg WP, Husebo BS, Caljouw MAA. Does paracetamol improve quality of life, discomfort, pain and neuropsychiatric symptoms in persons with advanced dementia living in long-term care facilities? A randomised double-blind placebo-controlled crossover (Q-PID) trial. BMC Med 2020;18:407.
[83] Vardeh D, Mannion RJ, Woolf CJ. Toward a mechanism-based approach to pain diagnosis. J Pain 2016;17:T50–69.
[84] Vogt BA. Cytoarchitecture and neurocytology of rabbit cingulate cortex. Brain Struct Funct 2016;221:3571–89.
[85] Vogt BA, Paxinos G. Cytoarchitecture of mouse and rat cingulate cortex with human homologies. Brain Struct Funct 2014;219:185–92.
[86] Vrinten DH, Hamers FF. "CatWalk" automated quantitative gait analysis as a novel method to assess mechanical allodynia in the rat; a comparison with von Frey testing. PAIN 2003;102:203–9.
[87] Wang LP, Li F, Wang D, Xie K, Wang D, Shen X, Tsien JZ. NMDA receptors in dopaminergic neurons are crucial for habit learning. Neuron 2011;72:1055–66.
[88] Wang X, Sun G, Feng T, Zhang J, Huang X, Wang T, Xie Z, Chu X, Yang J, Wang H, Chang S, Gong Y, Ruan L, Zhang G, Yan S, Lian W, Du C, Yang D, Zhang Q, Lin F, Liu J, Zhang H, Ge C, Xiao S, Ding J, Geng M. Sodium oligomannate therapeutically remodels gut microbiota and suppresses gut bacterial amino acids-shaped neuroinflammation to inhibit Alzheimer's disease progression. Cell Res 2019;29:787–803.
[89] Wu JJ, Lu YC, Hua XY, Ma SJ, Shan CL, Xu JG. Cortical remodeling after electroacupuncture therapy in peripheral nerve repairing model. Brain Res 2018;1690:61–73.
[90] Xu ZZ, Kim YH, Bang S, Zhang Y, Berta T, Wang F, Oh SB, Ji RR. Inhibition of mechanical allodynia in neuropathic pain by TLR5-mediated A-fiber blockade. Nat Med 2015;21:1326–31.
[91] Yang EJ, Mahmood U, Kim H, Choi M, Choi Y, Lee JP, Cho JY, Hyun JW, Kim YS, Chang MJ, Kim HS. Phloroglucinol ameliorates cognitive impairments by reducing the amyloid beta peptide burden and pro-inflammatory cytokines in the hippocampus of 5XFAD mice. Free Radic Biol Med 2018;126:221–34.
[92] Yuste R. Electrical compartmentalization in dendritic spines. Annu Rev Neurosci 2013;36:429–49.
[93] Zagrebelsky M, Holz A, Dechant G, Barde YA, Bonhoeffer T, Korte M. The p75 neurotrophin receptor negatively modulates dendrite complexity and spine density in hippocampal neurons. J Neurosci 2005;25:9989–99.
[94] Zang KK, Xiao X, Chen LQ, Yang Y, Cao QL, Tang YL, Lv SS, Cao H, Zhang L, Zhang YQ. Distinct function of estrogen receptors in the rodent anterior cingulate cortex in pain-related aversion. Anesthesiology 2020; 133:165–84.
[95] Zhang D, Yan X, She L, Wen Y, Poo MM. Global enhancement of cortical excitability following coactivation of large neuronal populations. Proc Natl Acad Sci U S A 2020;117:20254–64.
[96] Zhao Y, Sivaji S, Chiang MC, Ali H, Zukowski M, Ali S, Kennedy B, Sklyar A, Cheng A, Guo Z, Reed AK, Kodali R, Borowski J, Frost G, Beukema P, Wills ZP. Amyloid beta peptides block new synapse assembly by nogo receptor-mediated inhibition of T-type calcium channels. Neuron 2017; 96:355–72.e356.
[97] Zhuo M. Cortical excitation and chronic pain. Trends Neurosci 2008;31: 199–207.